Modeling dispersal of the Pearl River-derived sediment over the Shelf

Guang Zhang[1,2,3], Suan Hu[1,2,3], Xiaolong Yu[1,2,3], Heng Zhang[1,2,3], Wenping Gong[1,2,3]*

[1] School of Marine Sciences, Sun Yat-sen University, Zhuhai, 519082, China

[2] Guangdong Provincial Key Laboratory of Marine Resources and Coastal Engineering, Zhuhai, 519082, China

[3] Pearl River Estuary Marine Ecosystem Research Station, Ministry of Education, Zhuhai 519082, China

Corresponding author: Wenping Gong (gongwp@mail.sysu.edu.cn)

Abstract

This study employs the Coupled-Ocean-Atmosphere-Wave-Sediment-Transport (COAWST) modeling system to quantitatively assess the seasonal suspension, transport, and annual fate of Pearl River-derived sediment (riverine slow-settling single fine grains and high-settling flocs) on the northern continental shelf of the South China Sea (SCS). Following careful model validation, a series of sensitivity experiments were conducted to investigate the effects of tides, waves, background circulation, sediment settling velocity, critical shear stress, and sediment spin-up durations. The results reveal strong seasonal variations in sediment dynamics driven by the East Asian monsoon. During the wet summer, weaker hydrodynamic conditions promote the initial deposition of riverine sediment via the surface buoyant plume. In contrast, stronger winds and waves during winter enhance sediment resuspension and southwestward transport, particularly toward the Beibu Gulf. Spatially, approximately two-thirds of the annual Pearl River-derived sediment load is retained near the estuary. About 9% reaches the continental shelf east of the PRE, while similar proportions accumulate in the Beibu Gulf and south of Hainan Island. Sensitivity experiments highlight the distinct roles of different physical forcings: tidal dynamics strongly influence sediment behavior in the estuary, where the absence of tidal forcing reduces bottom shear stress, leading to increased local deposition and reduced offshore transport. Wave forcing plays a dominant role in sediment resuspension near the river mouth and along the coast, especially during winter. Excluding waves leads to greater sediment retention near the estuary and diminished

transport toward distant regions. Ambient circulation, particularly in summer, is essential for eastward sediment transport; when it is omitted, northeastward dispersal is greatly diminished. Model outcomes are also sensitive to sediment parameterization. Using non-seasonal critical shear stress for erosion increases wintertime sediment mobility east of the Leizhou Peninsula. Higher settling velocities decrease suspended sediment concentrations and promote near-source retention, limiting long-distance transport. Spin-up duration experiments indicate that Pearl River–derived sediment, which enters and accumulates in various regions of the model domain during the first year, continues to migrate southwestward in the second year under the influence of the mean annual flow field. In contrast, the spin-up duration of seabed sediment has little impact on the retentions of Pearl River–derived sediment on the shelf. Overall, this study reveals the transport pathway and fate of the Pearl River-derived sediment and provides a model-based assessment of its seasonal behavior and dispersal mechanisms on the northern SCS shelf. It identifies key physical drivers regulating sediment transport and deposition patterns, offering new insight into sediment fate in a monsoon-dominated shelf system.

This study employs the Coupled Wave-Ocean-Sediment Transport Model to quantitatively assess the seasonal suspension, transport, and annual fate of Pearl River-derived sediment on the northern South China Sea (SCS) continental shelf. After careful model validation, several sensitivity model simulations were conducted. Results reveal pronounced seasonal variations in sediment dynamics driven by the monsoonal climate. During the wet summer, calm conditions favor initial deposition

via the river plume, whereas stronger winter winds and waves resuspend and transport sediments into the Beibu Gulf. Spatially, 66.45% of the total sediment load is retained within the estuarine vicinity, 9.2% is deposited on the eastern continental shelf, and 8.86% and 10.3% accumulate in the Beibu Gulf and the area south of Hainan Island, respectively. Sensitivity experiments highlight the distinct roles of tidal forces, wave action, and background circulation in sediment transport and deposition. Tidal dynamics govern sediment behavior in the Pearl River Estuary, where neglecting tidal effects underestimates bottom shear stress, overestimates sediment deposition, and underestimates distal retention. Wave action dominates sediment resuspension at the river mouth, nearshore regions, particularly during high-energy winter periods. Excluding waves leads to overestimated deposition in these areas and underestimates accumulation in the Beibu Gulf. Background circulation is most influential in summer, with a strong northeastward current transporting sediments to the eastern shelf. Without this current, only 0.84% of sediments reach the eastern shelf, leading to an overestimation of distal deposition. The sediment model results are also highly sensitive to sediment parameterization and initial conditions. Neglecting seasonal variations in critical shear stress for erosion overestimates winter resuspension and erosion east of the Leizhou Peninsula, increasing distal retention. Higher settling velocities lower SSC while overestimating proximal retention and underestimating distal retention. Additionally, initial sediment conditions significantly impact sediment transport, with the retention of pre-existing sediment leading to further offshore transport. However, the model is relatively insensitive to the initial bed grain

size distribution. This study provides a comprehensive assessment of Pearl River-derived sediment dynamics and highlights key physical mechanisms governing sediment fate in the northern SCS.

Keywords

Riverine sediment transport; Sediment retention; Numerical modeling; Pearl River Estuary

1. Introduction

The transport process of suspended sediment from river source to ocean sink is an important link in the global material cycle (Geyer et al., 2004; McKee et al., 2004; Kuehl et al., 2016; Liu et al., 2016; Cao et al., 2019). Much of the riverine sediment is trapped on the shallow shoals in estuaries, while the rest is transported by buoyant river plume out of the estuary (Meade, 1969; Burchard et al., 2018; Zhang et al., 2019). The riverine sediment carried by the buoyant river plume has a significant impact on the water quality, ecology, and geomorphology of the estuaries and continental shelves (Wright and Coleman, 1973; Turner and Millward, 2002).

The transport and deposition of riverine sediments from river source to estuarine, coastal, and shelf environments are controlled governed by diverse various physical processes, including tidal forces, wave action, and shelf circulation dynamics (Dalyander et al., 2013; Gao and Collins, 2014; Xu et al., 2016; Warner et al., 2017; Zang et al., 2019; Wang et al., 2020). Tides play a critical role in sediment transport dynamics in estuarine and shelf regionssediment transport dynamics, as spring tides typically produce higher bed shear stress, enhanced sediment resuspension, and

98   greater offshore sediment transport flux compared to neap tides (Bever and

99   MacWilliams, 2013; Zhang et al., 2019; Wang et al., 2020). In nearshore regions,

100   wave-induced bed shear stress ~~is~~ often exceeds current-induced stress by an order of

101   magnitude ~~higher than that generated by currents~~ (Xue et al., 2012; Dalyander et al.,

102   2013). Furthermore, wave-driven sediment resuspension frequently surpasses~~exceeds~~,

103   and is often several times greater than, the peak levels achieved by current-induced

104   resuspension (Sanford, 1994; Harris et al., 2008; Brand et al., 2010; Xu et al., 2016).

105   In shelf regions, ~~shelf~~ circulation patterns significantly modulate ~~influence~~ sediment

106   transport, with the magnitude of along-shelf transport substantially exceeding the

107   cross-shelf component in most areas ~~locations~~ (Nittrouer and Wright, 1994; Geyer et

108   al., 2004; Gao and Collins, 2014; Wang et al., 2020).

109   Furthermore, sediment properties, including settling velocity (Xia et al., 2004;

110   Chen et al., 2010; Cheng et al., 2013), critical shear stress for erosion (Dong et al.,

111   2020), and bed grain size distribution (Xue et al., 2012; Bever and MacWilliams,

112   2013), significantly influence sediment transport dynamics and

113   deposition/resuspension processes. Settling velocity can influence the location of

114   sediment depocenters, with higher settling velocities leading to more proximal

115   entrapment and vice versa (Ralston and Geyer, 2017). Similarly, critical shear stress

116   for erosion can affect the resuspension of deposited sediment, with higher critical

117   shear stress resulting in less resuspension and more deposition especially during neap

118   tides and weak wind wave periods (Dong et al., 2020; Choi et al., 2023).

119   A comprehensive understanding of sediment transport and deposition from river

source to ocean sink requires the integrated consideration of both physical forcing

factors and inherent sediment characteristics. Here, we present the transport and

deposition of the Pearl River-derived sediments on the continental shelf as a case

study. The Pearl River, ranking as China's second-largest river in terms of freshwater

discharge (Hu et al., 2011), forms the Pearl River Estuary (PRE) in its lower reaches

(Figures 1 and S1). Its freshwater and sediment discharge are primarily delivered

through eight major outlets (Figure S1b; Wu et al., 2016; Zhang et al., 2019; Zhang et

al., 2025), forming distinct buoyant plumes that extend across the northern South

China Sea (SCS) shelf (Zhang et al., 2025). The present average annual (2001-2022)

freshwater and riverine sediment loads are 2.74×10^{11} m^3 and 2.84×10^7 tons,

respectively, as reported by the Ministry of Water Resources of the People's Republic

of China (http://www.mwr.gov.cn/sj/#tjgb). The distribution of these inputs shows

significant seasonal variability: approximately 80% of the freshwater and 95% of the

sediment load are transported during the wet summer season (April to September),

while the remaining portion is discharged during the dry winter season (Xia et al.,

2004).

The northern SCS, shaped by the East Asian Monsoon, displays marked seasonal

contrasts, featuring winter monsoon winds averaging 7-10 m s^{-1} and summer winds

typically below 6 m s^{-1} (Su, 2004; Ou et al., 2009). This seasonal shift drives coastal

currents: northeastward in summer and southwestward in winter (Gan et al., 2009;

Gan et al., 2013). Beyond the coastal zone, the consistent SCS Warm Current

(SCSWC) flows northeastward along the shelf break and inner continental slope

toward the Taiwan Strait, originating near Hainan Island and persisting year-round, even during the winter northeast monsoon, across a remarkable distance of 600-700 km to the southern tip of the Taiwan Strait (Su, 2004; Yang et al., 2008).

The PRE is situated in the central part of the northern South China Sea boundary, positioned between the Taiwan Banks and Hainan Island. The PRE has a micro-tidal and mixed semi-diurnal regime, with daily inequality in the range and in the time between the high and low tides (Mao et al., 2004). The neap and spring tides alternately influence the water elevation downstream of the estuary, with tidal ranges varying from approximately 0.7 m during neap tides to over 2 m during spring tides (Chen et al., 2016; Gong et al., 2018b). The PRE and the nearby shelf exhibit strong seasonal variation in water column stability and are highly stratified during the wet summer season, while the PRE becomes partially mixed or vertically well-mixed during the dry winter season (Dong et al., 2004). Offshore of the PRE region, wave conditions display distinct seasonal patterns: the waves are mild during summer, and become stronger during winter, marked by larger southeasterly waves (Gong et al., 2018a; Gong et al., 2018b; Zhang et al., 2021).

Previous studies have focused on sediment transport within the PRE (Zhang et al., 2019; Zhang et al., 2021; Ma et al., 2024). Most Pearl River-derived sediments are deposited within the estuary, and neglecting tidal effects can lead to higher overestimating deposition rates and lowerwhile underestimating offshore sediment flux when compared to those with tides (Hu et al., 2011). The depositional dynamics of sediments from different PRE outlets are shaped regulated by outlet location,

topography, and tidal conditions, with neap tides favoring sediment accumulation on

shoals and spring tides driving erosion and enhancing offshore sediment transport

(Zhang et al., 2019). Waves further intensify both lateral trapping within the PRE and

offshore sediment transport (Liu and Cai, 2019; Zhang et al., 2021).

However, numerical studies on the transport of the Pearl River-derived sediments

across the continental shelf remain scarce, even amidst the widespread adoption of

computer modeling approaches. Previous research on the distribution of these

sediments has primarily relied on analyses of seismic profiles, gravity cores, and

laboratory-based radiometric dating of sediment samples (Ge et al., 2014; Liu et al.,

2014; Cao et al., 2019; Lin et al., 2020; Chen et al., 2023). Outside the PRE, gravity

core and seismic survey data were used to examine the Holocene sedimentary

processes, revealing two distinct mud depo-centers: an eastward proximal depo-center

extending southeastward from the PRE's mouth and a southwestward distal mud belt

(Ge et al., 2014; Liu et al., 2014; Chen et al., 2023). However, seismic and drilling

data cannot confirm that the Pearl River sediment can be transported to the Beibu

Gulf (Ge et al., 2014). Due to the lack of sufficient gravity core samples and seismic

data, it is difficult to quantitatively attribute the sediment in the Beibu Gulf to the

Pearl River-derived sediment (Cao et al., 2019). Afterward, Lin et al. (2020) used the

^{226}Ra—^{238}U and ^{232}Th—^{238}U endmembers model based on measurements of

radionuclides in the surface sediment samples. They found that approximately 15% of

the surface sediment in the nearshore area of the Beibu Gulf originates from the PRE

region. However, their studies only address the proportion of the PRE sediment in the

surface sediment of the Beibu Gulf, without directly indicating the seasonal transport

pathways, flux, and annual deposition ~~mechanisms~~ of the sediment from the Pearl

River.

A gap persists in understanding how physical processes (such as tides, waves, and

ambient circulations) and sediment characteristics (such as critical shear stress for

erosion, settling velocity) and sediment initial conditions influence the seasonal

suspension, transport, and annual deposition of the Pearl River-derived sediment on

the shelf. Specifically, this study focuses on sediment classes 4 and 5 in Table 1,

which represent the Pearl River-derived components: slow-settling single fine grains

(Class 4) and fast-settling flocs (Class 5), in contrast to the background seabed

sediments represented by classes 1 to 3. To address this~~In this study~~, we utilize

numerical modeling, complemented by extensive collection of field observations and

seabed grain size distribution data for model calibration and validation—a highly

effective approach for exploring mechanisms and testing hypotheses derived from

limited observational datasets. This study aims to systematically investigate the

dispersal dynamics~~focused on the processes~~ of the Pearl River-derived sediment

~~suspension, transport, and deposition~~ over the northern South China Sea ~~continental~~

shelf, with particular emphasis on the following objectives~~. Several specific questions~~

~~addressed in this paper include~~:

(1) Quantify ~~What are~~ the seasonal dispersal and annual deposition ~~patterns~~ of the

Pearl River-derived sediment (classes 4 and 5 in Table 1) over the continental shelf~~?~~.

(2) Examine the relative roles of ~~How do~~ physical ~~processes~~forcings (tides, waves,

208 and ambient circulations), sediment characteristics (critical shear stress for erosion,

209 settling velocity) and (Pearl River-derived versus Seabed) sediment spin-up durations

210 ~~initial conditions~~ ~~influence~~ on the dispersal of the Pearl River-derived sediment~~?~~.

211
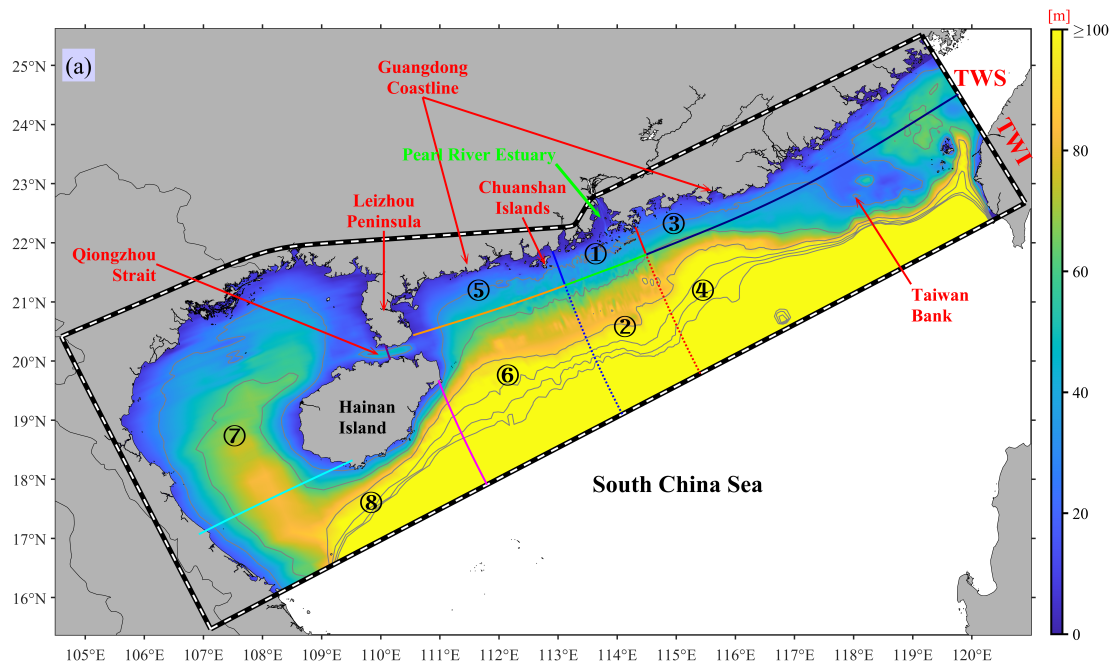
Figure 1. Bathymetry (shading) and isobath contours of the study area, with the ROMS/SWAN model grid domain outlined by black-to-white dashed lines. Circled numbers ①-⑧ denote the eight regions: "Proximal", "Southern", "Eastern", "Southeastern", "Western", "Southwestern", ~~Beibu~~ "Gulf", and "Distal" regions, as defined by transects and detailed in Section 2.1~~4.2~~. The abbreviations TWI and TWS mean Taiwan Island and Taiwan Strait, respectively. The gray contours represent 30-180 m isobaths at 30 m intervals, a consistent feature maintained in all subsequent figures that include these isobath contours.

221

2. Methods

2.1 Model coupling

This study employed the Coupled Ocean Atmosphere Wave Sediment Transport (COAWST, version 3.4) modeling system (Warner et al., 2005; Warner et al., 2008; Warner et al., 2010), which includes a Model Coupling Toolkit (MCT) to facilitate data exchange among different modules (Jacob et al., 2005; Larson et al., 2005). The COAWST system consists of several modeling components, mainly comprises a hydrodynamic module (Regional Ocean Modeling System; ROMS) (Shchepetkin and McWilliams, 2005; Haidvogel et al., 2008), an atmospheric module (Advanced Research Weather Research and Forecasting; WRF) (Skamarock et al., 2005), a wave module (Simulating Waves Nearshore; SWAN) (Booij et al., 1999), and a sediment transport module (Community Sediment Transport Modeling System; CSTM) (Warner et al., 2008).

In this study, we established a coupling between ROMS, SWAN, and CSTM. The model grid covered covers the northern continental shelf of the South China Sea, including the PRE (Figure 1). The regional model was configured with 170×482 horizontal grid cells, with horizontal resolution varying from approximately 0.1 km near the PRE to about 10 km at outer open boundaries (Hu et al., 2024; Zhang et al., 2025). The model grid bathymetry data was obtained from nautical charts compiled by the China Maritime Safety Administration and the General Bathymetric Chart of the Oceans (GEBCO) (Weatherall et al., 2015). The vertical grid used a terrain-following S Sigma coordinate system (Song and Haidvogel, 1994) with 20

244 layers and a stretching transformation for higher resolution near the surface and

245 bottom, with stretching parameters of θ_s=3.0 and θ_b=3.0, respectively (Song and

246 Haidvogel, 1994). For model validations, please refer to the Supplementary Material

247 (Supplement Figures S1-S10).

248   To improve the understanding of the spatial-temporal variabilities in the riverine

249 sediment dispersal, and the estimation of the fate of the Pearl River sediment during

250 the wet summer season, dry winter season, and throughout the year, we partitioned the

251 model domain into eight distinct regions delineated by various transects as illustrated

252 in Figure 1. The division criteria are mainly based on the distance from the estuary

253 and the natural separation by the Leizhou Peninsula and Hainan Island (Figure 1).

254 These regions include:

255   ① Proximal region: Proximity to the estuary,

256   ② Southern region: Located deeper in the southern part of the estuary,

257   ③ Eastern region: Eastern side of the estuary, closer to the shoreline,

258   ④ Southeastern region: Further offshore on the eastern side of the estuary,

259   ⑤ Western region: Western side of the estuary, closer to the shoreline,

260   ⑥ Southwestern region: Offshore on the western side of the estuary,

261   ⑦ Gulf region: Mainly the Beibu Gulf,

262   ⑧ Distal region: South of the Hainan Island.

263   By dividing the model domain into these delineated regions, we calculated the

264 riverine sediment flux for each transect, thereby determining the total riverine

265 sediment volume retained in each region.

266

2.2 ROMS model setup

For the ROMS model, we utilized the Generic Length Scale turbulence closure scheme (Warner et al., 2005) for vertical turbulence parameterization. The method of Smagorinsky (1963) was employed to calculate the horizontal eddy viscosity and diffusivity. The Flather and Chapman boundary conditions were applied to barotropic current and water elevation at open boundaries, respectively (Flather, 1976; Chapman, 1985). Meanwhile, the open-boundary conditions for temperature, salinity, and sediment concentration were imposed by radiation methods (Orlanski, 1976; Raymond and Kuo, 1984). Surface forcing (including wind, net shortwave radiation, air temperature, atmospheric pressure, specific/relative humidity, and rain, etc.) data were sourced from the Climate Forecast System Reanalysis of the National Centers for Environmental Prediction (NCEP) (Saha et al., 2014), with a temporal resolution of 1 h and a spatial resolution of $0.3° \times 0.3°$. Water level and current open-boundary conditions comprised two components: tidal and subtidal. The tidal component was obtained from the Oregon State University Tidal Prediction Software database (Egbert and Erofeeva, 2002), while the subtidal component was interpolated from the HYbrid Coordinate Ocean Model (HYCOM) outputs (Chassignet et al., 2007).

2.3 Wave model setup

The SWAN model was executed and coupled to the same grid as the ROMS model (Warner et al., 2010). It was driven by surface atmospheric forces, real-time water level, and current fields from the ROMS and boundary reanalysis data. Wave

boundary conditions were specified using nonstationary wave parameters from outputs of the NOAA WAVEWATCH III global ocean wave model solutions (Tolman et al., 2016). Information was exchanged at 15-minute intervals to introduce wave-current interaction (WCI) between the ROMS and SWAN models (McWilliams et al., 2004; Kumar et al., 2012). This exchange included significant wave height (Hsig), surface peak wave period, mean wave direction and length, wave energy dissipation, and the percentage of breaking waves from SWAN to ROMS, as well as water level and current from ROMS to SWAN.

Additionally, the wave-current bottom boundary module based on Madsen (1994), incorporated into COAWST, was activated to simulate the wave-current bottom boundary layer. The vortex force module of wave forces was also activated to compute the wave-induced momentum flux, utilizing the method proposed by McWilliams et al. (2004) and implemented in COAWST by Kumar et al. (2012). The bottom friction was computed based on a logarithmic velocity profile (Warner et al., 2008).

2.4 Specifications of riverine input and sediment model

The freshwater discharge for the Pearl River was specified at the northern boundary using daily measured data from the Pearl River Water Resources Commission, while downstream precipitation within the Pearl River Basin was neglected. The full simulation model was initialized on the first day of January 2016 using temperature, salinity, and current fields interpolated from the HYCOM model, and it concluded on March 31, 2018. More than one year of hydrodynamic and

sediment spin-up is sufficient to achieve appropriate seabed sediment particle size distribution, as well as stable circulation and thermohaline fields. This study primarily analyzes the last 12 months, specifically from April 1, 2017, to March 31, 2018. This year is was selected because the freshwater discharge and sediment load of the Pearl River closely approximated the average values of the past two decades, with a runoff of 3.35×10^{11} m^3 and a sediment load of 3.45×10^7 tons, closely resembling the averages from 2001 to 2022.

Since the daily riverine sediment loads were unavailable, we modified the previous research results on sediment rating curves (Zhang et al., 2012) to suit for our study, as expressed by

$$y = 0.00002263x^{1.792} \tag{1}$$

where y is the Pearl River-derived suspended sediment concentration (mg L^{-1}), x is the Pearl River freshwater discharge rate (m^3 s^{-1}). Based on this relationship, the total amount of Pearl River sediment input over our 12-months study period (Figure. 3b) was 34.52 million tons, aligning closely with the annual load reported in 2017 by the Pearl River Water Resources Commission. The riverine sediment input, derived from the river discharge, was allocated across the eight outlets along the north boundary (Figure S1b) based on the distribution approach of Hu et al. (2011).The subsequent step involved involves establishing the proportion of seabed sediment particle size components. Sediments are typically categorized into three grain-size classes: clay (0-4 μm), silt (4-63 μm), and sand (63-2000 μm), as outlined by Shepard (1954). Data on sediment particle size composition for the northern continental shelf of the South

332   China Sea and the PRE area were acquired through multiple voyage observations

333   (Zhang et al., 2013; Zhang et al., 2019). Furthermore, publicly available data from

334   published literature were compiled (Gao et al., 2007; Kirby et al., 2008; Gao et al.,

335   2010; Huang et al., 2013; Liu et al., 2014; Wang et al., 2014; Wang et al., 2015; Wang

336   et al., 2016; Ge et al., 2017; Lu et al., 2017; Zhong et al., 2017; Yang et al., 2018; Ge

337   et al., 2019). Finally, component distribution data for different particle size classes of

338   seabed sediment were obtained from a total of 1981 measured stations (Figure 2a-c).

339

340
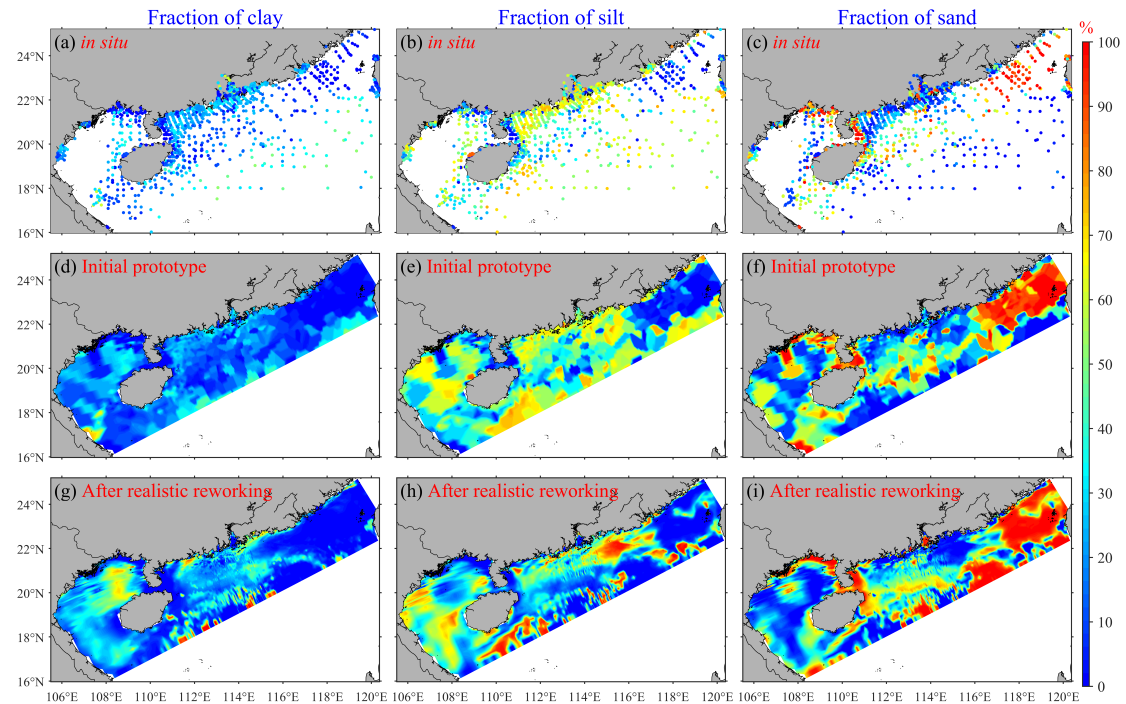
341   **Figure 2.** Row 1 presents the spatial distribution patterns of seabed sediment fractions

342   derived from 1981 sampling sites, while Row 2 demonstrates the initial spatial

343   distribution prototype of seabed sediment fractions developed based on the

344   observational data presented in Row 1. Row 3 shows the spatial distribution patterns

345   of seabed sediment fractions following the completion of spin-up phase in the Control

346 run case on April 1st, 2017, with Columns 1, 2, and 3 representing the fractions of

347 clay, silt, and sand, respectively.

348

349 As illustrated in Figure 2a-c, the measured stations exhibit a widespread

350 distribution, offering comprehensive coverage of the entire northern continental shelf

351 of the South China Sea, including the PRE. Particularly dense distribution is observed

352 in the PRE and the coastal areas of western Guangdong. These regions represent the

353 primary scope of transport and deposition associated with the Pearl River-derived

354 sediment. Hence, the stations utilized in this study well represent the distribution of

355 bed sediment particle size components in these study areas. It is evident that among

356 the stations in the offshore area of the northern continental shelf of the South China

357 Sea, silt dominates, followed by clay, while sand with the largest particle size is the

358 least abundant. This suggests a significant presence of terrestrial sediment or Pearl

359 River sediment in the offshore area of the northern continental shelf of the South

360 China Sea. It should be noted that the lack of in situ grain size distribution data in

361 specific regions of the model domain, especially in the Beibu Gulf area, may lead to

362 uncertainties in sediment transport predictions. We will address these limitations and

363 quantify their potential errors in the discussion part of this study.

364 To derive the component proportions of the initial prototype field on the model

365 grid, this study employed the Kriging method (Krige, 1951), widely recognized for

366 spatially interpolating various types of observational data. The sediment distribution

367 pattern obtained through interpolation (Figure 2d-f) closely resembles the original

368   1981 measured sediment particle size distribution patterns (Figure 2a-c), suggesting

369   the suitability of this interpolation method for the study area.

370   The initial prototype field underwent a 15-month spin-up period (from January 1,

371   2016, to March 31, 2017), during which the bottom sediment composition ~~it~~ evolved

372   under ~~was adjusted by realistic reworking, incorporating~~ realistic hydrodynamic~~s~~

373   forcings from the ~~in~~ ROMS, SWAN, and CSTM models. ~~This adjustment allowed for~~

374   ~~the redistribution of seabed sediment fractions based on the modeled hydrodynamics.~~

375   This method has been utilized in numerous previous studies, including those by Bever

376   et al. (2009), van der Wegen et al. (2010), and Zhang et al. (2021). ~~The realistic~~

377   ~~spin-up greatly reduced the irregularities and prepared a more suitable seabed~~

378   ~~sediment particle size distribution field for subsequent simulations than the initial~~

379   ~~prototype (Figures 2d f vs. 2g i).~~ This process allows the initially idealized sediment

380   distribution to evolve under realistic dynamic forcings, including tides, waves, and

381   currents, thereby minimizing unreasonable spatial patterns introduced by the Kriging

382   interpolation method. Such unreasonable spatial patterns may arise due to limitations

383   in the number, representativeness, and timing of field sediment samples relative to the

384   model start date. As a result, the sediment field after the spin-up period (Figures 2g–i)

385   exhibits spatial patterns that are more physically plausible and better aligned with the

386   hydrodynamic conditions of the study region.

387   During both the 15-month spin-up period and the subsequent 12-month formal

388   model experiments (see Section 2.6 and Table 2)~~simulations~~, the CSTM utilized five

389   sediment classes (Table 1), ~~which~~ represent~~ing~~ a range of sediment sizes and

characterics.~~,~~ These included ~~including~~ three types of seabed sediments (clay, silt, and sand, corresponding to sediment Classes 1 to 3~~the first three categories of sediments~~ in Table 1) and two types of Pearl River-derived sediments (Class 4 and Class 5 in Table 1).~~the sum of the fourth and fifth categories of sediments in Table 1, namely the~~ The riverine sediments consisted of slow-settling single fine grains (Class 4) and high-settling flocs (Class 5), which were delivered into the model domain during both the 15-month spin-up period and the subsequent 12-month formal model experiments). The riverine flocs correspond to the flocculated fractions of clay and silt, whereas the single fine grains represent the non-flocculated components within the Pearl River-derived sediments, following the setting of Bever and MacWilliams (2013). To clarify, at the start of the 12-month formal model experiments, the retained Pearl River-derived sediments (Classes 4-5 in Table 1) that entered the model during the 15-month spin-up period were added as Class 1 and Class 2, respectively, to avoid contaminating the data analysis of the formal experiments. This approach allows for a better distinction between Pearl River sediment and seabed sediment, enabling separate analysis of the suspension, transport, and deposition of Pearl River-derived sediment (Harris et al., 2008; Zhang et al., 2019). ~~To clarify, the initial setup of the formal model simulations excludes the retained riverine sediment (Class 4 and Class 5 in Table 1) from the model domain during the spin-up period. The riverine flocs correspond to the flocculated fractions of clay and silt, whereas the single fine grains represent the non-flocculated components within the Pearl River-derived sediments, following the setting of~~ Bever and MacWilliams (2013).~~.~~ Specifically, the fractions of

412   the two types of Pearl River-derived sediments were set at 40% and 60%, respectively,

413   following Zhang et al. (2019) and Zhang et al. (2021). The parameters for all five

414   sediment classes are summarized in Table 1. Sediment density, porosity, and erosion

415   rate for all sediment classes were set to 2650 kg m^{-3}, 0.672 (Zhang et al., 2019; Zhang

416   et al., 2021), and 1×10^{-4} kg m^{-2} s^{-1} (Ralston et al., 2012), respectively. The settling

417   velocity (w_s), critical shear stresses for erosion (τ_{ce}), and other parameters were set

418   following previous studies or were based on model calibration (Ralston et al., 2012;

419   Warner et al., 2017; Zhang et al., 2019; Dong et al., 2020; Zhang et al., 2021; Cao et

420   al., 2025).

421   Our model configuration incorporates seasonal variations in τ_{ce}, supported by

422   multiple lines of evidence from field observations, laboratory experiments, and

423   numerical analyses (Dong et al., 2020; Cao et al., 2025). Previous studies have

424   established a distinct seasonal pattern in the PRE, with winter τ_{ce} values significantly

425   exceeding those in summer. Dong et al. (2020)'s laboratory experiments using the

426   UMCES-Gust Erosion Microcosm System (U-GEMS) on 2017-winter sediment

427   samples yielded a τ_{ce} of 0.26 Pa, which effectively reproduced observed suspended

428   sediment concentration (SSC) in winter simulations. However, this value proved

429   excessive for summer conditions, when ~~where~~ a τ_{ce} of 0.15 Pa provided better

430   agreement with field observations in summer simulations, indicating a

431   winter-to-summer τ_{ce} ratio of 1.73. Recent 2020-summer in situ measurements by Cao

432   et al. (2025) using a benthic quadrapod-mounted 3D Profiling Sonar revealed a

433   two-layer erosion threshold system: a surface "fluffy layer" with $\tau_{ce} = 0.06$ Pa

overlying a consolidated seabed with $\tau_{ce} = 0.13$ Pa. The latter value aligns with Dong et al. (2020)'s summer calibration, suggesting that Dong et al. (2020)'s laboratory measurements, potentially affected by sediment consolidation during sample transport, might have missed the lower τ_{ce} of the surface fluffy layer. Based on these consistent findings, we implemented a seasonal τ_{ce} adjustment factor of 1.73 (winter/summer) in our model configuration (Table 1).

Table 1. CSTM model Sediment Properties

Source	Seabed			Pearl River	
Class	1	2	3	4	5
Sediment Type	Clay	Silt	Sand	Single grains	Flocs
w_s (mm s^{-1})	0.02[c]	1.2	57[d]	0.005[c]	0.6
Summer τ_{ce} (Pa)	0.14[e]	0.03	0.27[d]	0.15[abef]	0.05[abe]
Winter τ_{ce} (Pa)	0.24[f]	0.05[f]	0.47[df]	0.26[abf]	0.09[abf]
Fraction	Spatially variable, see Figure 2g-i			40%[ab]	60%[ab]

[a]Zhang et al. (2019), [b]Zhang et al. (2021), [c]Calibrated, [d]Warner et al. (2017), [e]Cao et al. (2025), and [f](Dong et al., 2020).

Sediment Type	Clay	Silt	Sand	single grains	flocs
w_s (mm s^{-1})	0.02[e]	1.2[e]	57[d]	0.005[e]	0.6[e]
Summer τ_{ce} (Pa)	0.14[cg]	0.03[e]	0.27[d]	0.15[abfg]	0.05[abcg]
Winter τ_{ce} (Pa)	0.24[ef]	0.05[ef]	0.47[df]	0.26[abf]	0.09[abcf]
Fraction	Spatially variable, see Figure 2g-i			40%[ab]	60%[ab]

[a]Zhang et al. (2019), [b]Zhang et al. (2021), [c]Ralston et al. (2012), [d]Warner et al. (2017), [e]Calibrated, [f](Dong et al., 2020), and [g]Cao et al. (2025).

2.5 Wet and dry season regimes

The study area exhibits pronounced seasonal variability, which can be distinctly categorized into two primary seasons (Dong et al., 2004; Su, 2004; Liu et al., 2014; Zhang et al., 2021). This seasonal classification is supported by multiple environmental parameters, including river freshwater discharge, riverine sediment load (Figure 3a), wind patterns (Figure 3b), air temperature (Figure 3c), and modelled wave conditions (Figure 3d-f) at a representative site (21.5°N, 114°E; corresponding to station W1 in Figure S1a, located immediately south of the PRE). The meteorological data for wind and air temperature were obtained from the NCEP reanalysis dataset, while wave parameters were derived from numerical model simulations. These comprehensive indicators collectively characterize the distinct seasonal patterns observed in the study area (Figure 3). The entire year (from April 1, 2017, to March 31, 2018) is typically divided into two main seasons: wet summer

463   (from April 1, 2017, to September 30, 2017) and dry winter (from October 1, 2017, to

464   March 31, 2018).

465   During the wet summer season, freshwater discharge tends to be notably high,

466   often exceeding 10,000 $m^3 s^{-1}$ and reaching a maximum of 53,000 $m^3 s^{-1}$, with an

467   average value of 15,266 $m^3 s^{-1}$. This discharge constitutes a significant portion of the

468   entire year, accounting for 72.06% of the annual total. During this period, the river

469   carries a substantial sediment load of 32.85 megatons, constituting 95.17% of the total

470   annual sediment transport. Prevailing winds predominantly blow from the south. For

471   example, Figure 3b depicts the average monthly wind vector direction during the

472   summer months as northward, with weak southeasterly winds in April, May, and

473   September, and moderate southeasterly winds in July. June and August experience

474   moderate southwesterly winds. The 2 m height air temperatures typically range

475   between 20℃ and 30℃. The daily average Hsig remains relatively low, with the

476   monthly average Hsig less than 1 m. The wave propagation direction is generally

477   consistent with the wind direction, being easterly in April and May, and southerly

478   from June to September.

479   In stark contrast, the dry winter season demonstrates markedly lower runoff,

480   typically falling below 10,000 $m^3 s^{-1}$, with an average value of 5,953 $m^3 s^{-1}$. The

481   sediment load during this period is significantly reduced to merely 1.67 megatons,

482   marking a substantial decrease compared to the wet summer season. Prevailing winds

483   during the dry winter are predominantly northeasterly, with relatively high wind

484   speeds. Except for moderate wind intensity in March, the monthly average wind speed

485 in other months exceeds 5 m s^{-1}. The 2 m height air temperatures typically range

486 between 10℃ and 25℃ during this season. The wave propagation direction aligns

487 with the prevailing northeasterly winds of the season, predominantly northeasterly.

488

489
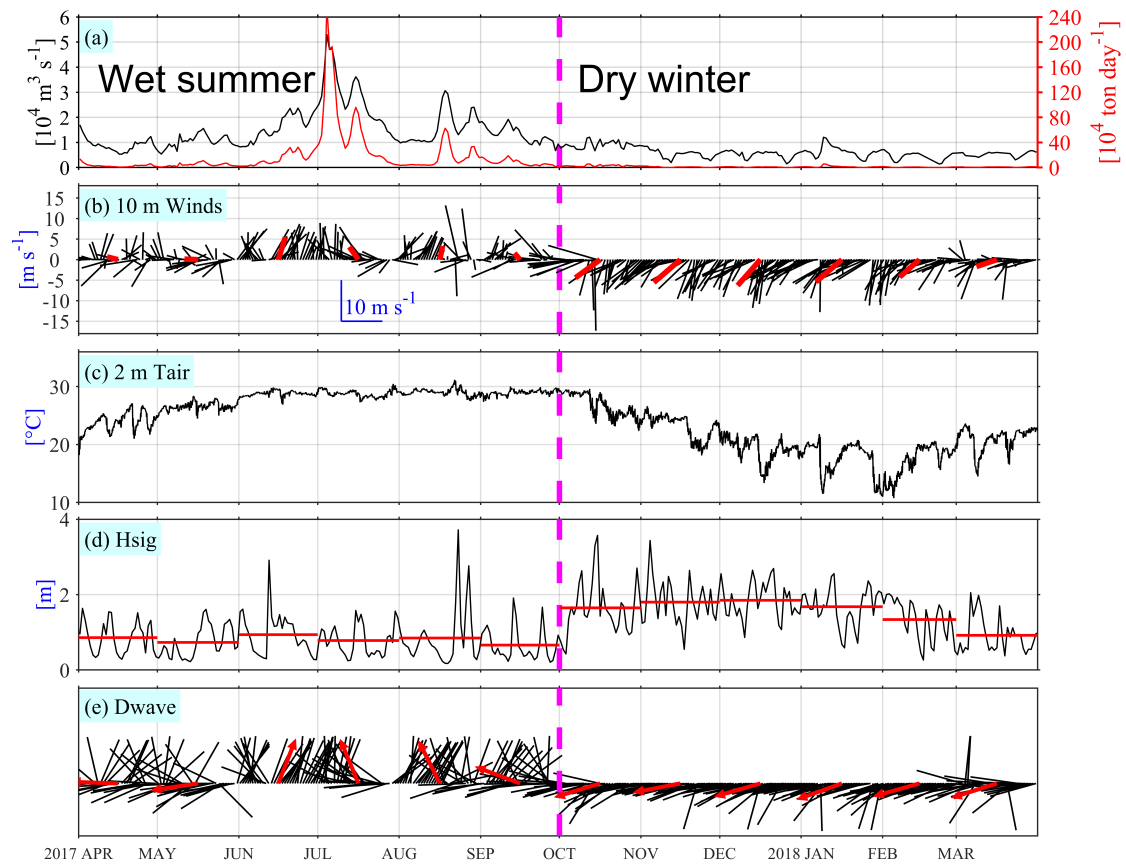
490 **Figure 3.** Time series of (a) the daily Pearl River freshwater discharge and sediment

491 load, (b) daily (black vectors) and monthly (red vectors) averaged 10-meter height

492 winds, (c) hourly 2-meter height air temperature, daily (black) and monthly (red)

493 averaged (d) significant wave height (Hsig, lines) and (f) wave propagation direction

494 (vectors) weighted by Hsig^2. Two distinct seasons are delineated by the dashed

495 magenta line.

496

2.6 Model experiments

To assess the relative importance of tides, waves, ambient shelf currents and residual water levels, seasonal variation in critical shear stress for erosion, the settling velocity, and the spin-up duration of Pearl River-derived sediment (Classes 4-5 in Table 1) initial conditions in the transport and dispersal of Pearl River-derived sediments, we conducted seven simulation experiments (Table 2). In all experiments, we implemented the Charnock approach within COAWST's bulk air-sea flux parameterization scheme to calculate surface wind stress using the NCEP 10-m wind product (Charnock, 1955; Fairall et al., 1996), ensuring consistency in wind stress forcing across all simulations.

Exp 1 (the **Control** run) incorporated all the aforementioned forcing agents (including winds) and accounted for the seasonal variation in critical shear stress for erosion, with the winter critical shear stress for erosion set to be 1.73 times of that in summer. Exp 2 (**NTS** hereafter) was identical to Exp 1 but excluded tides, while Exp 3 (**NWS** hereafter) excluded waves. In Exp 4 (**NAS** hereafter), waves, tides, and the seasonal variation in critical shear stress for erosion were included, but the shelf current and residual water levels were was omitted (i.e., no subtidal circulation forcing at open boundaries) to examine the influence of the South China Sea circulation. Exp 5 (NVS hereafter) replicated the setup of Experiment 1, but with one modification: it used a constant critical shear stress for erosion (τ_{ce}) across both seasons, specifically adopting the summer τ_{ce} value from Table 1 throughout the simulation (i.e., no seasonal adjustment between winter and summer).Then, Exp 5

(**NVS** hereafter) was identical to Exp 1, except that it did not account for the seasonal variation in critical shear stress for erosion, keeping the winter and summer values the same. Exp 6 (**DSV** hereafter) was identical to Exp 1, except that it set a double sediment settling velocity of the Exp 1. Finally, to assess the model's sensitivity to the spin-up duration of Pearl River-derived sediment, particularly regarding the retention of riverine sediments in both the water column and the seabed, we adopted the sediment distributions (Classes 1 to 5) from the Control run on March 31, 2018, as the alternative initial conditions for the Cycle experiment (designated as Exp 7, **Cycle** hereafter). This setup carries over the full year's evolution of riverine sediment transport and deposition from the Control run (Exp 1), including changes in all sediment classes, into the start of Exp 7. As a result, Exp 7 mainly evaluates how the presence of previously deposited riverine sediments influences subsequent sediment transport estimates. Finally, to evaluate the model's sensitivity to sediment initial conditions, particularly focusing on the retention of riverine sediments within the water column and the seabed, we utilized the Control run's Class 1-5 sediment suspensions and depositions recorded on March 31, 2018, as alternative initial conditions for the five sediment classes. This configuration was implemented in the second control simulation, designated as Exp 7 (**Cycle** hereafter). Consequently, this setup introduces a full year's worth of Pearl River derived sediment suspensions and depositions into the model domain at the start of the **Cycle** experiment.

Table 2. Experiment Settings

Experiments	Tides	Waves	Ambients	τ_{ce}	w_s	Re-run
Exp 1 (Control)	✓	✓	✓	Variable	Original	✕
Exp 2 (NTS)	✕	✓	✓	Variable	Original	✕
Exp 3 (NWS)	✓	✕	✓	Variable	Original	✕
Exp 4 (NAS)	✓	✓	✕	Variable	Original	✕
Exp 5 (NVS)	✓	✓	✓	Constant	Original	✕
Exp 6 (DSV)	✓	✓	✓	Variable	Double	✕
Exp 7 (Cycle)	✓	✓	✓	Variable	Original	✓

The term 'Ambients' denotes ambient shelf currents and residual water levels. Variable indicates simulations employing seasonally varying τ_{ce} values (from Table 1), while 'Constant' refers to runs using exclusively the summer τ_{ce} value throughout the entire experiment. 'Original' designates cases utilizing the settling velocities specified in Table 1, whereas 'Double' indicates simulations with these values doubled."

In all experiments, we implemented the Charnock approach within COAWST's bulk air sea flux parameterization scheme to calculate surface wind stress using the NCEP 10 m wind product (Charnock, 1955; Fairall et al., 1996), ensuring consistency in wind stress forcing across all simulations.

3 Results

3.1 Seasonal hydrodynamics and transport patterns of the Pearl River-derived sediment transport patterns

555   We quantified the spatial distributions of seasonal mean wind stress, Hsig, wave

556   bottom orbital velocity (WBOV), and bottom shear stress for both the wet summer

557   and dry winter periods (as defined in Section 2.5). These distributions serve as

558   representative hydrodynamic conditions for typical summer and winter scenarios,

559   respectively (Figure 4).

560   During summer, the prevailing winds predominantly originate from the south,

561   with the average wind stress generally below 0.03 Pa, except in the eastern coastal

562   waters of Hainan Island, where localized values reach up to 0.05 Pa (Figure 4a). In

563   contrast, during the dry winter season, the prevailing winds shift to a northeasterly

564   direction, resulting in generally higher average wind stress compared to summer

565   (Fig.ure 4b), with values typically exceeding 0.1 Pa in areas deeper than 40 m and

566   surpassing 0.2 Pa in the offshore eastern Guangdong Coast near the Taiwan Bank (see

567   Figure 1).

568   Corresponding to the seasonal wind stress (Figures 4a-b), the seasonally averaged

569   wave characteristics in the PRE and the adjacent northern continental shelf of the

570   South China Sea exhibit significant seasonal variations (Figures 4c-d).

571   During the wet summer season, the Hsig in the studied areathese areas is

572   relatively low, with waves predominantly coming from the southeast (Figure 4c). The

573   seasonal average Hsig across the entire shelf remains below 1 m, with areas deeper

574   than 60 m showing Hsig values above 0.8 m, while in shallower nearshore regions

575   (water depth < 20 m), Hsig is less than 0.6 m (Figure 4c). Corresponding to the lower

576   Hsig in the wet summer, the seasonally-averaged WBOV is also relatively small,

577 generally less than 1 cm s^{-1} in areas deeper than 40 m, except in some nearshore

578 shallow water regions where it reaches up to 10 cm s^{-1} (Figure 4e). The

579 seasonally-averaged bottom shear stress during the wet summer is relatively high in

580 the PRE, nearshore regions, and the Taiwan Bank, where tidal dissipation is strong

581 (Figure 4g).

582 In the dry winter season, the Hsig increases significantly compared to the wet

583 summer, with waves primarily coming from the northeast, although refraction occurs

584 in some nearshore regions, changing the wave direction to southeasterly (Figure 4d).

585 The area with water depths exceeding 60 m has a Hsig greater than 1.5 m, while in the

586 20-meter depth region, the Hsig reaches approximately 1 m (Figure 4d). Compared to

587 the wet summer, the WBOV increases significantly in the PRE mouth and many

588 nearshore regions, reaching up to 10-20 cm s^{-1} (Figure 4d). The average bottom shear

589 stress on the continental shelf outside the estuary also increases significantly during

590 the dry winter compared to the wet summer (Figure 4f).

591
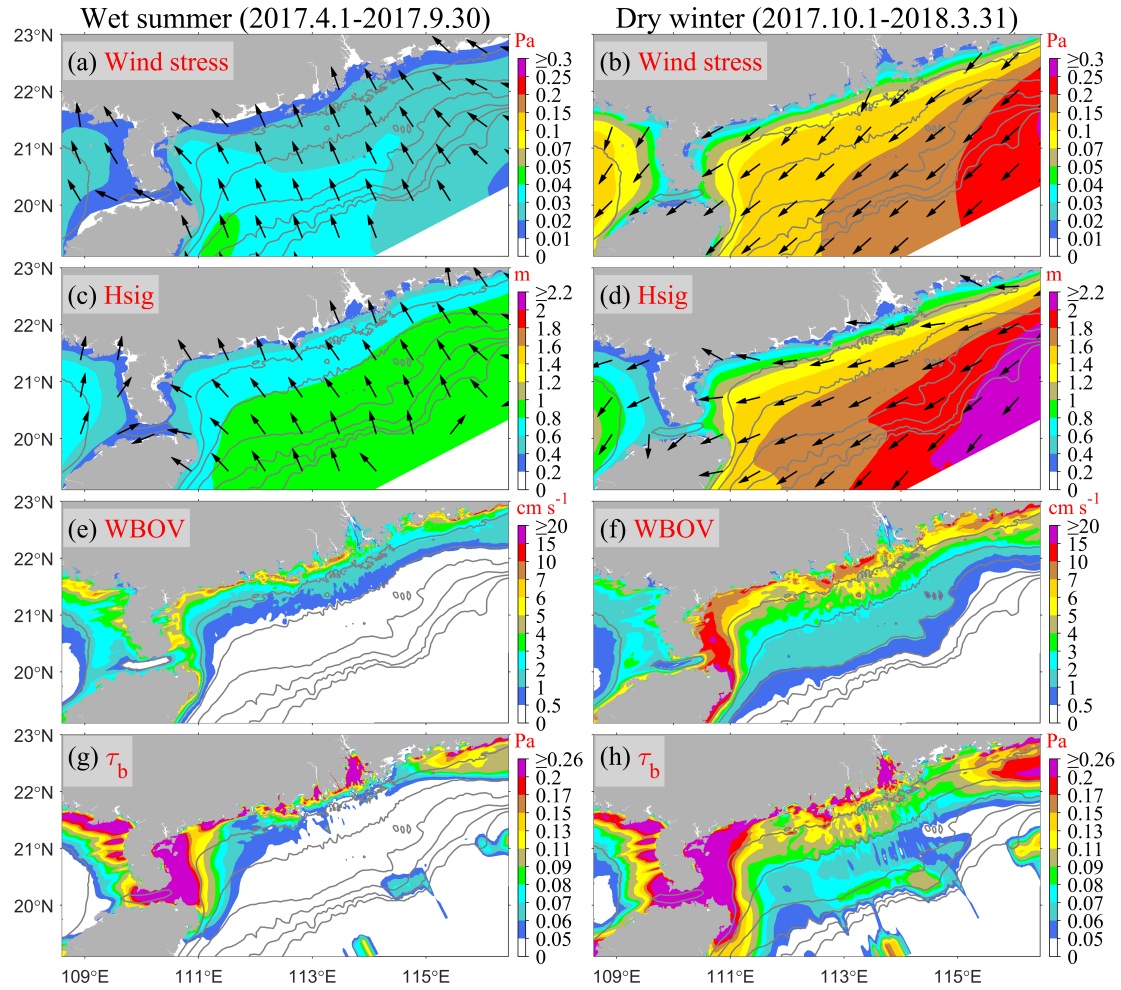
Figure 4. The patterns of variables averaged for the wet summer season (April 1st to September 30th, 2017; Column 1) and the dry winter season (October 1st to March 31st, 2018; Column 2) in the Control case. Row 1 (a-b) depicts wind stress (color) and direction (vectors), Row 2 (c-d) shows Hsig (color) and propagation direction (vectors) weighted by Hsig², Row 3 (e-f) presents wave bottom orbital velocity (WBOV), and Row 4 (g-h) displays bottom shear stress magnitude.

The patterns of residual sediment dispersal, flux, and deposition over the simulation period provide clear information on the mechanisms for sediment redistribution on both annual and seasonal timescales. The following~~This~~ section

603   presents a detailed analysis of the seasonally averaged fields of salinity, flow, riverine

604   SSC, depth-integrated riverine sediment flux, and riverine sediment deposition

605   patterns during the wet summer season (Figure 5) and dry winter season (Figure 6) on

606   the continental shelf.

607   During the wet summer season, when freshwater discharge is high and water

608   column stratification is strongthe Pearl River discharges a significant amount of

609   freshwater and sediment (Figure 3a), riverine SSC ("riverine" means only Pearl

610   River-derived sediment, classes 4-5 in Table 1, as follows) is primarily influenced by

611   advection from the buoyant river plumeresulting in an extensive expansion of the

612   river plume (salinity less than 33.5 in Figure 3a, as follows) into the shelf sea,

613   primarily in the surface layer (Figures 5a-b), high SSC regions closely align with the

614   buoyant plume, as sediment is efficiently transported by the low-salinity,

615   high-momentum freshwater outflow (Figures 5a-d). The buoyant river plume extends

616   both northeastward and southwestward along the coastline (Figure 5a). Due to the

617   influence of southerly winds (Figure 4a) and ambient shelf currents, the extent of the

618   buoyant river plume extending northeastward is significantly higher than that

619   extending southwestward.

620   In terms of riverine sediment suspension, its estuarine turbidity maxima

621   (ETM)maximum turbidity zone (~100 mg L^{-1}) is situated in the shallow water area

622   within the estuary (water depth < 10 m) (Figure 5c-d). Beyond the estuary, suspended

623   riverine sediment disperses across the shelf through the buoyant river plume. Further

624   away from the estuary, its distribution aligns with that of the buoyant river plume,

with concentrations diminishing as dispersal distance increases. The depth-integrated ~~Integrating the~~ advective horizontal flux (without including vertical processes such as settling, resuspension, or diffusion, which are handled separately within the model) of riverine sediment ~~vertically~~ offers a clear indication of the primary net transport pathway of the riverine sediment (Figure 5e). The riverine sediment exhibits both southwestward and northeastward fluxes (Figure 5e). Southw~~W~~estward coastal transport can extend as far as the Leizhou Peninsula and Hainan Island. On the eastern side, the northeastward transport extends toward the Taiwan Bank. However, the primary transport pathway there is diverted southward (Figure 5e) due to the obstruction caused by summer upwelling near the Guangdong east coast (Chen et al., 2017a; Chen et al., 2017b), as evidenced by the cross-shore current in the bottom layer (Figure 5b). The southwestward transport pathway follows the region where the water depth is shallower than 30 m, with a riverine sediment flux of 10–20 $g\ m^{-1}\ s^{-1}$~~$g^{-1}\ m\ s^{-1}$~~. In contrast, the northeastward transport pathway occurs in the 30–60 m depth range, but the riverine sediment flux is below 10 $g\ m^{-1}\ s^{-1}$~~$g^{-1}\ m\ s^{-1}$~~. Throughout the wet summer season, substantial amounts of riverine sediment are deposited near the estuary (Figure 5d), particularly leading to notably high deposition of riverine sediment near the river mouth (> 100 mm). Outside the estuary, the thickness of riverine sediment is comparatively lower, but it can reach approximately ~0.5 mm during the wet summer season in certain areas off the ~~coast of~~ western Guangdong coast.

646

647
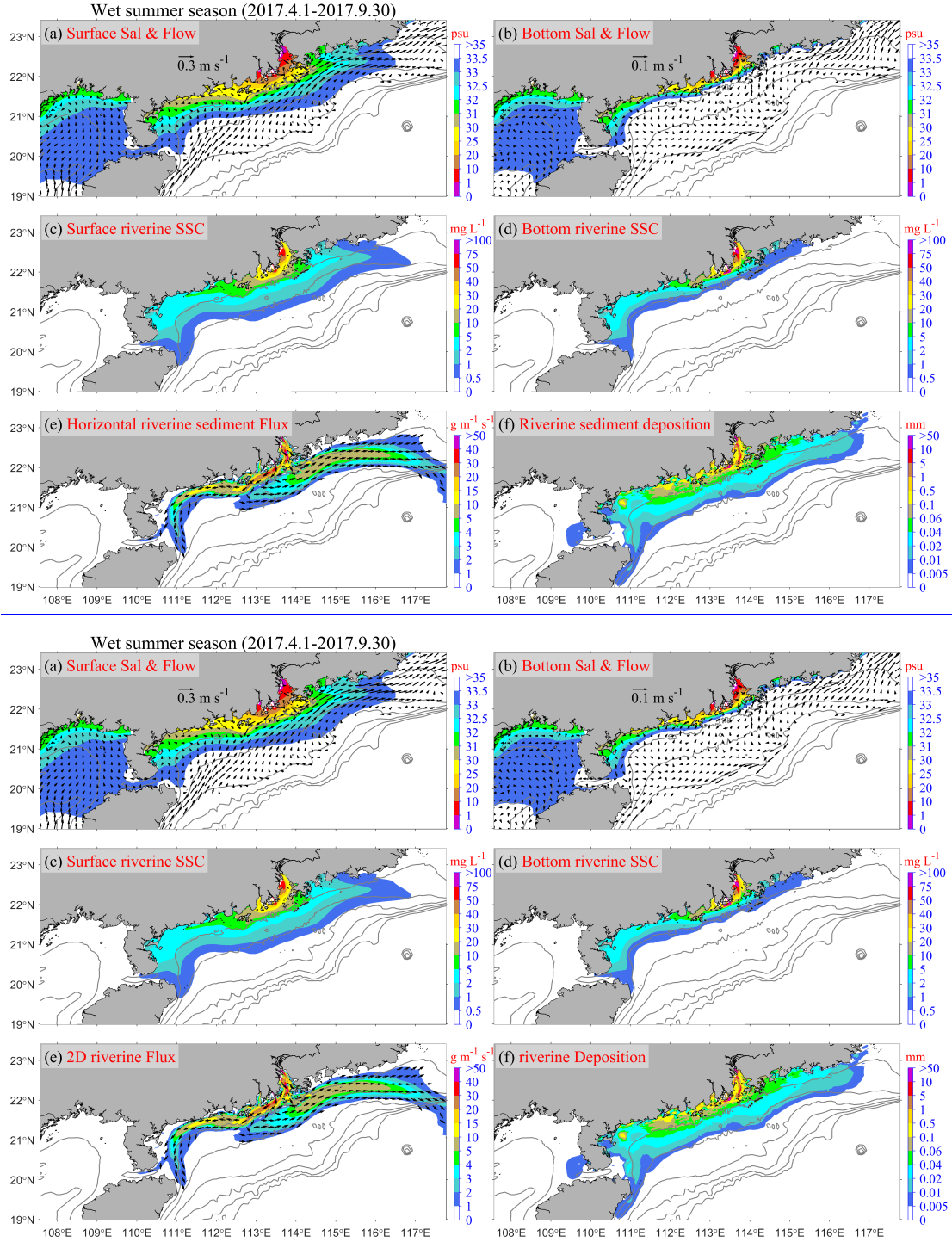
Figure 5. Patterns averaged over the entire wet summer season in the Control case: (a) surface and (b) bottom salinity (color, psu) and flow (arrows, m s^{-1}); (c) surface and (d) bottom riverine (classes 4 and 5 in Table 1, as follows) SSC (mg L^{-1}); (e) depth-integrated horizontal riverine sediment transport rate (color, g m^{-1} s^{-1}) and

direction (arrows); and (f) riverine sediment deposition thickness (mm) on the seabed during the wet summer season (mm). Flow vectors in regions with water depths exceeding 100 m are masked for clarity.

In contrast, during winter, when river discharge is low and vertical mixing is more intense, the correlation between the buoyant plume and riverine SSC is much weaker, and the riverine SSC is largely governed by resuspension processes driven by strong northeasterly winds and waves, rather than by freshwater transport. During the dry winter season, runoff from the Pearl River significantly decreases compared to the wet summer (as indicated in Figure 3a), accompanied by strong northeasterly winds (Figure 4b). Consequently, the The expansion of the Pearl River buoyant plume is constrained to the southwestward direction by strong northeasterly winds only(Figure 6a), resulting in a narrow cross-shore width of the buoyant plume and the formation of a strong horizontal salinity gradient (i.e., a salinity front, particularly within the 30–33.5 psu range shown in Figure 6a) outside the estuary (Figure 6a). Flow velocity increases is increased near this the salinity front, facilitating theallowing river plume to extend westward extension of the buoyant plume through the Qiongzhou Strait into the "Gulf" regionBeibu Gulf. With sediment load during winter nearly negligible, the suspended concentration of riverine sediment The riverine SSC is significantly lower than in compared to the wet summer: in the ETM zone inside the PRE, riverine SSC falls from roughly 100 mg L^{-1} in summer to about 10 mg L^{-1}, while on the offshore shelf, it decreases from approximately 5 mg L^{-1} to around 2 mg L^{-1} (Figures 6c-db vs.

674 5c-d). ~~In areas beyond the estuary, it is typically less than 3 mg L^{-1}, whereas inside the~~

675 ~~estuary, it is around ~5 mg L^{-1}.~~ During the dry winter, following the ~~transport path of~~

676 ~~river plume~~ coastal current, the riverine suspended sediment primarily moves

677 southwestward along the coast, deflecting southward along the topography near the

678 Leizhou Peninsula (Figure 6c). It then bifurcates near the east entrance of the

679 Qiongzhou Strait, with one branch continuing into the "Gulf" region~~Beibu Gulf~~, and

680 the other one ~~branch~~ proceeding southward along the east coast of Hainan Island.

681 Stronger winds and waves in the dry winter lead to the resuspension of a considerable

682 amount of riverine sediments, originally deposited in "Proximal", "Western", and

683 "Eastern" regions ~~estuaries and shelf seas~~ during summer. The resuspended sediments

684 are then transported to coastal bays as well as to the sides and rears of the islands

685 (Figure 6d). Additionally, a portion of the riverine sediment transported to the "Gulf"

686 region~~Beibu Gulf~~ gets deposited on the seabed during the dry winter season.

687
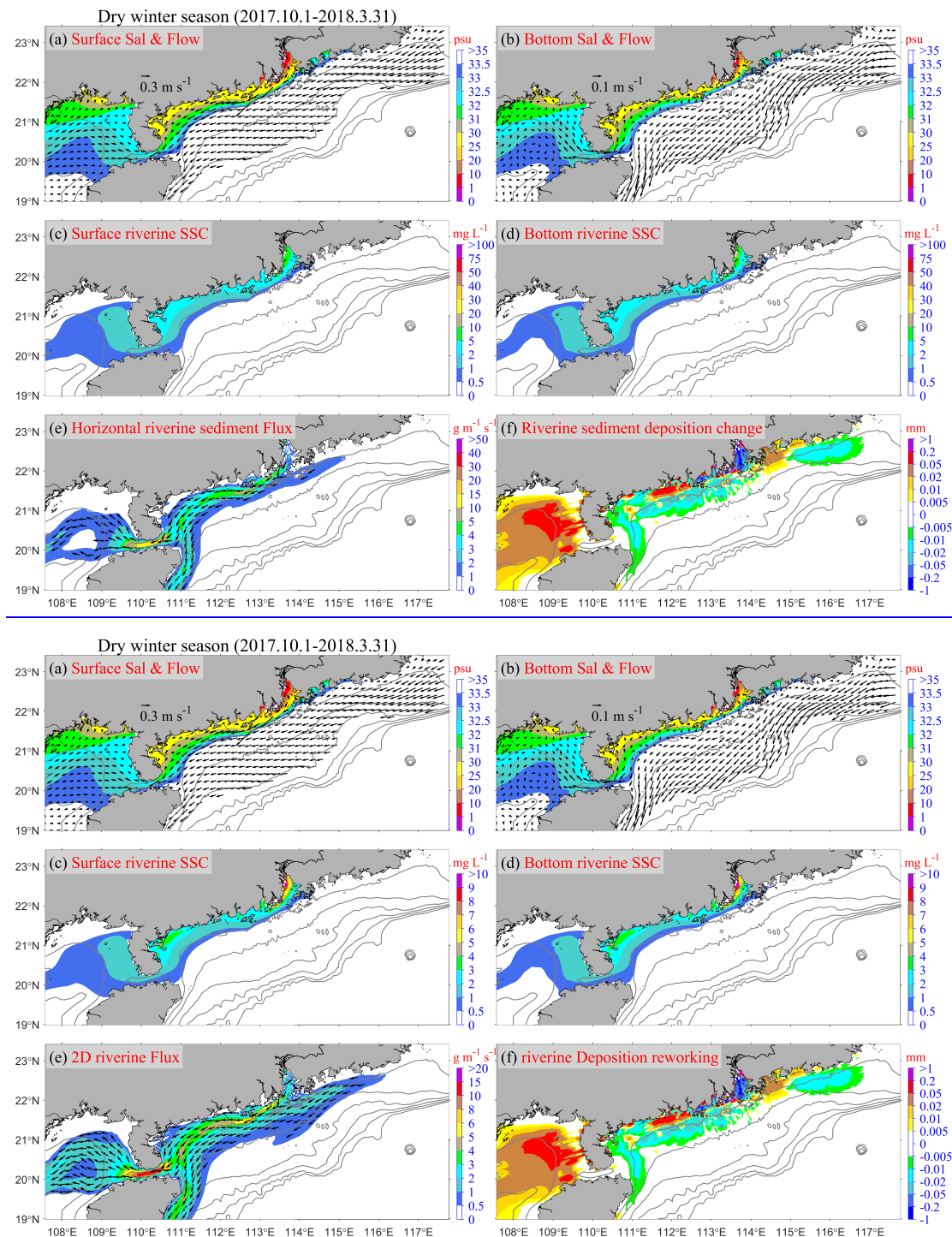
Figure 6. Same as Figure 5, but for the dry winter season in the Control case. Notably,

(f) illustrates the changes in riverine sediment (classes 4 and 5 in Table 1) deposition

on the seabed at the end of the dry winter season compared to the end of the wet

summer season.

3.2 Riverine sediment budgets and annual deposition over the shelf

~~To improve the understanding of the spatial-temporal variabilities in the riverine sediment dispersal, and the estimation of the fate of the Pearl River sediment during the wet summer season, dry winter season, and throughout the year, we partitioned the model domain into eight distinct regions delineated by various transects as illustrated in Figure 1. The division criteria are mainly based on the distance from the estuary and the natural separation by the Leizhou Peninsula and Hainan Island. These areas include:~~

~~① Proximal region: Proximity to the estuary,~~

~~② Southern region: Located deeper in the southern part of the estuary,~~

~~③ Eastern region: Eastern side of the estuary, closer to the shoreline,~~

~~④ Southeastern region: Further offshore on the eastern side of the estuary,~~

~~⑤ Western region: Western side of the estuary, closer to the shoreline,~~

~~⑥ Southwestern region: Offshore on the western side of the estuary,~~

~~⑦ Gulf region: Mainly the Beibu Gulf,~~

~~⑧ Distal region: South of the Hainan Island.~~

~~By dividing the model domain into these delineated regions, we calculated the riverine sediment flux for each transect, thereby determining the total riverine sediment volume retained in each region. Additionally,~~ We present the sediment fluxes and retention amounts in different regions. Figure 7a-c illustrates the proportion of riverine sediment retention budget within each region, expressed as a

percentage of the total annual river sediment input, for the wet summer season, the

dry winter season, and the entire year under the Control run case, respectively.

Meanwhile, Figure 7d illustrates the annual deposition over the shelf.

The retention of Pearl River sediment on the continental shelf exhibits significant

seasonal variations (Figures 7a-c). During summer (characterized by high discharge

and low wind/waves), the PRE and continental shelf receive 95.17% of the annual

sediment load from the Pearl River (Figures 3a and 7a). Approximately two-thirds of

this sediment is retained in the "Proximal" region (Figure 7a). Additionally, influenced

by the prevailing southerly winds and northeastward shelf ~~background~~ circulation,

13.01% of the annual sediment load is retained ~~on the shelf east of the PRE,~~

~~specifically~~ in the "Eastern" and "Southeastern" regions (Figure 7a). Meanwhile, the

shelf west of the PRE (⑤−⑧ regions) retains 15.87% of the annual load, with the

"Western" region being the primary receiver, accounting for 8.48% (Figure 7a). Only

0.92% and 2.3% of the annual load enter the "Gulf" and "Distal" regions, respectively,

during summer (Figure 7a). The "Southern" region retains a mere 1.~~33~~22% of the

sediment (Figure 7a). In winter (characterized by low discharge and energetic

winds/waves), the PRE and the continental shelf receive only 4.83% of the annual

sediment load (Figures 3a and 7b). The sediment distribution during this season is

primarily a result of the dynamic reworking of the sediments of summer deposition

(Figure 7b). While the "Proximal" region continues to receive sediment, with a 1.38%

increase in retention, the ~~other five regions~~②−⑥ regions ~~east of the Leizhou~~

~~Peninsula and Hainan Island~~ experience a decrease in sediment retention. This

sediment is predominantly transported and retained in ~~to~~ the more distant "Gulf" and

"Distal" regions (Figure 7b). The annual sediment budget reveals that 66.45% of the

Pearl River sediment is retained in the "Proximal" region (Figure 7c). Additionally,

9.2% is retained in the "Eastern" and "Southeastern" regions~~on the shelf east of the~~

~~estuary~~ (Figure 7c), primarily during summer (Figures 7a vs. 7c), while 24.12% is

retained on the shelf west of the PRE ~~estuary~~(⑤−⑧ regions), with the majority

~~deposited~~ in the "Gulf" and "Distal" regions ~~distal regions of the Beibu Gulf and south~~

~~of Hainan Island~~, mainly during winter (Figures 7b vs. 7c).

The annual deposition thickness of the Pearl River sediments, as illustrated in

Figure 7d, reveals significant ~~proximal~~ deposition within ~~and near~~ the "Proximal"

region~~estuary~~, with many areas exceeding 10 mm despite winter resuspension and

transport. Additionally, deposition on the ~~inner shelf (water depth <60 m) to the~~

"Eastern" region~~east of the PRE~~ reached a magnitude of 0.1 mm, while the western

shelf of the PRE ("Western" and "Gulf" regions) exhibited significantly greater

accumulation. For instance, the deposition west of the Chuanshan Islands reached a

magnitude of 0.5 mm. In the "Gulf"~~Beibu Gulf~~ region, deposition was primarily

concentrated in the northeastern part ~~of the gulf~~, extending southwestward along the

30-60 m isobaths. Sediments transported southwestward along the east~~ern~~ coast of

Hainan Island and retained in the "Distal" regions did not predominantly settle on the

seabed due to the greater water depth but remained largely suspended in the water

column.

760
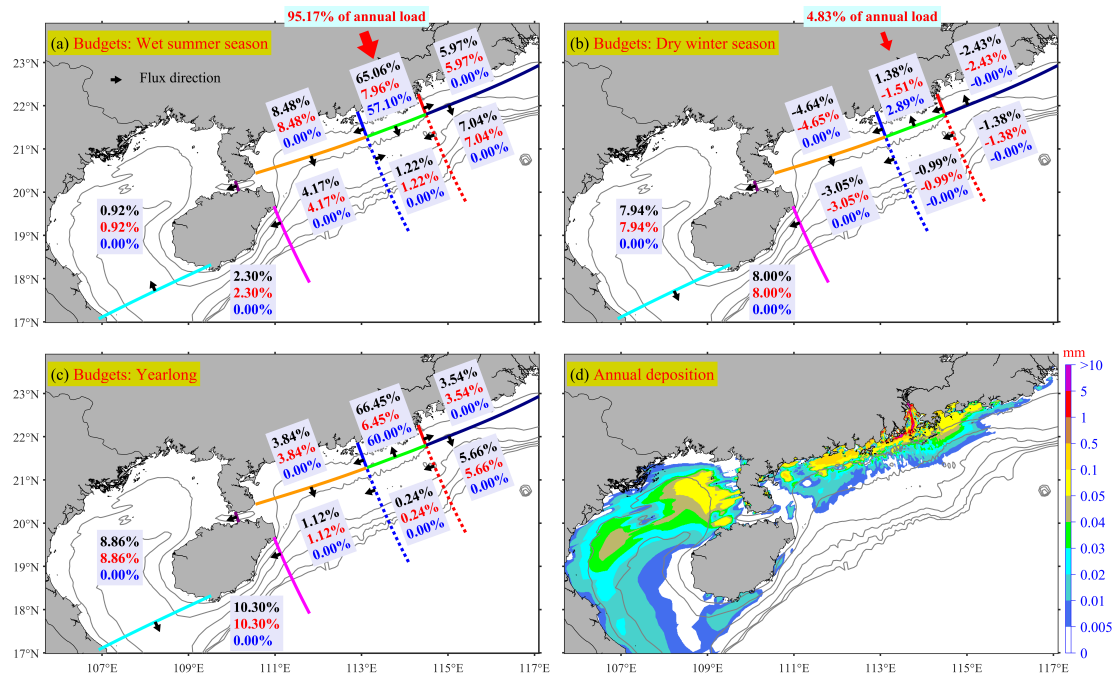
Figure 7. Riverine sediment (classes 4 and 5 in Table 1) retention budget percentages at eight regions (see Figure 1) during (a) the wet summer season, (b) the dry winter season, and (c) the entire year in the Control run case. (d) the annual deposition patterns spanning from April 1st, 2017, to March 31st, 2018 in the Control Run. All percentages displayed in the figure are relative to the annual riverine sediment load (see Figure 3a). The black percentage values represent the combined total of riverine sediment Class 4 and Class 5, while the red and blue values denote sediment Class 4 and Class 5, respectively. Arrows indicate the direction of net riverine sediment flux at each transect during the specified period.

770

780

781 **3.3 Model sensitivity experiments: relative roles of physical processes,**

782 **sediment properties, and ~~initial condition~~spin-up duration s**

783   Six sensitivity simulations, namely Exp 2-7 (NTS, NWS, NAS, NVS, DSV, and

784 Cycle), were conducted (Table 2). As the latter three experiments do not impact

785 hydrodynamics, we focus on presenting the seasonal mean differences in bottom shear

786 stress between the Control run and the first three cases (NTS-Control, NWS-Control,

787 NAS-Control) for both summer and winter (Figure 8).

788 ~~Tidal and wave forces significantly influence bottom stress.~~ In the NTS case,

789 ~~where tidal forces were excluded, the underestimation of~~ bottom shear stress is ~~was~~

790 reduced relative to the Control run by a similar amount in both summer and winter

791 due to the minimal seasonal variation in tidal intensity. This reduction ~~underestimation~~

792 primarily occurs ~~occurred~~ in the PRE, around the Taiwan Bank, and near the Leizhou

793 Peninsula (Figures 8a-b). In contrast, in the NWS case, the reduction in bottom shear

794 stress is greater~~which excluded wave forces, showed a greater underestimation~~ in

795 winter than in summer, reflecting the intense seasonal variability of wind and wave

796 activities (Figures 3b, 3d-e, and 4a-f). Unlike the NTS case, the NWS-induced

797 decrease occurs mainly ~~case mainly underestimated the bottom stress~~ in the nearshore

798 areas outside the PRE, although similar declines are also found~~though it similarly~~

799 ~~underestimated the bottom stress~~ around the Taiwan Bank and along the eastern side

800 of the Leizhou Peninsula (Figures 8c-d). For the NAS case, ~~where ambient shelf~~

801 ~~currents and residual water levels at the model boundaries were excluded,~~ the impact

802 on bottom stress is ~~was~~ minimal compared to the NTS and NWS cases. The effect is

803 ~~was~~ almost negligible on the inner shelf at depths less than 100 m, with widespread

804 impacts generally below 0.02 Pa. Some pronounced deviations ~~overestimations~~ are

805 ~~were~~ noted in localized deeper areas near the southern boundary ~~boundaries~~of the

806   domain (Figures 8e-f). These deviations, likely arising from boundary condition

807   effects, are situated far from the Pearl River-derived sediment distribution areas

808   (Figures 5-6). Consequently,~~probably being artifacts, but these changes in bottom~~

809   ~~stress, being distant from the Pearl River sediment distribution areas,~~ they do not

810   influence ~~did not affect~~ the dynamics of the Pearl River-derived sediment transport

811   over the continental shelf (Figures 8e-f).

812
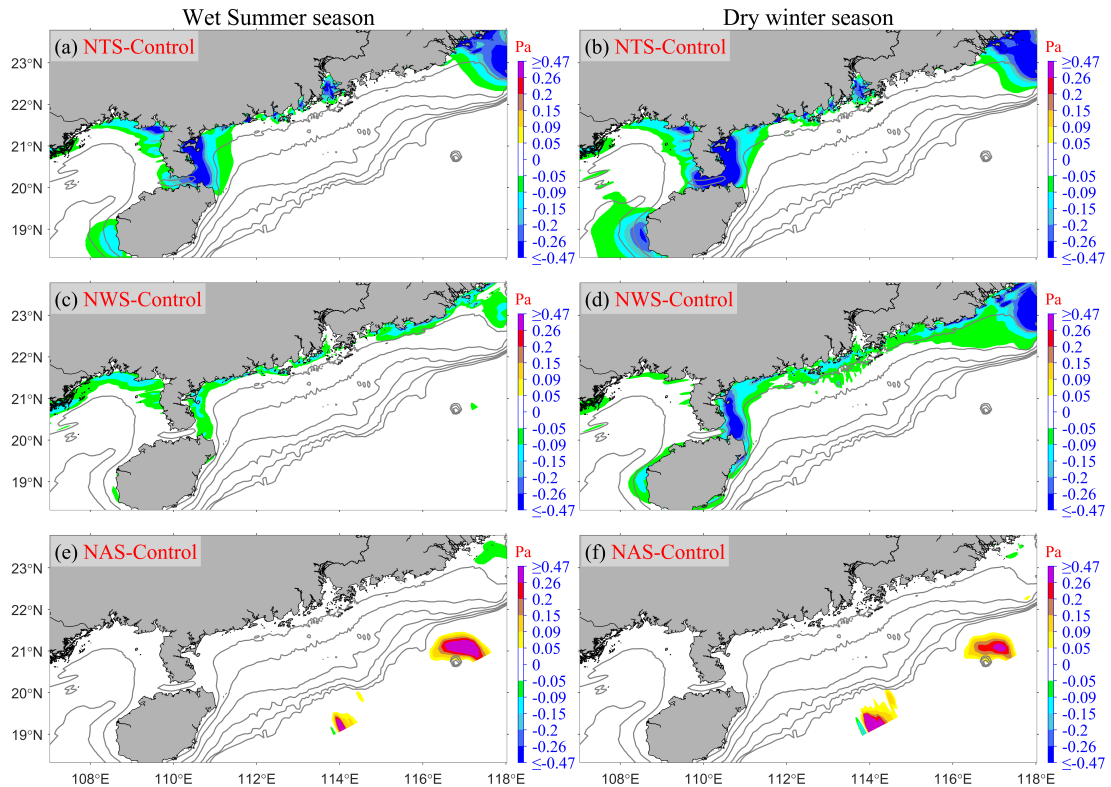
Figure 8. The seasonal mean differences in bottom shear stress between the Control

run and the following cases: (a-b) NTS (NTS minus Control), (c-d) NWS (NWS

minus Control), and (e-f) NAS (NAS minus Control). The first column represents the

wet summer season, while the second column corresponds to the dry winter season.

~~Following the bottom shear stress analysis (Figure 8)~~Then, we analyzed seasonal riverine sediment transport and deposition patterns ("riverine" means only the Pearl River-derived sediment, classes 4-5 in Table 1, as follows) by comparing the control run with six sensitivity experiments (NTS-Control, NWS-Control, NAS-Control, NVS-Control, DSV-Control, and Cycle-Control) (Figures 9-11). The study focuses on the Pearl River-derived sediment dynamics, indicated by surface circulation and riverine SSC distribution patterns (Figures 5 and 6). Specifically, Figures 9 and 10 present seasonal surface currents and SSC differences between control and sensitivity runs, complemented by deposition pattern differences in Figure 11.

~~For the NTS case versus~~ Compared to the Control case, the NTS case demonstrates that while tides significantly enhance ~~affected~~ bottom stress (Figures 8a-b) but have ~~had~~ minimal impact on the mean circulation (Figures 5a, 6a, and 9a-b), and their~~. The~~ exclusion ~~of tides substantially reduced~~ reduces bottom shear stress by over 0.2 Pa in the PRE and near the Leizhou Peninsula~~, weakening sediment resuspension~~. Consequently, increased deposition of the Pearl River-derived sediments occurs ~~occurred~~ inside the PRE, its adjacent areas, and on both sides of the Leizhou Peninsula (Figure 11a). During summer, riverine SSC notably ~~decreased~~ decreases in the ①−⑥ regions~~PRE and the inner shelf east of the Leizhou Peninsula~~ (Figure 9a). This reduction pattern ~~persisted~~ persists in winter, particularly in the PRE and on both sides of the Leizhou Peninsula (Figure 9b).

~~In the NWS case with waves excluded, like~~ Like the NTS, NWS ~~had~~ has a relatively minor impact on circulation (Figures 5a, 6a, and 9c-d). However, NWS

underestimated the nearshore bottom stress (Figures 8c-d). This leads led to more

Pearl River-derived sediment being deposited outside the PRE and in the nearshores

of "Western" and "Eastern" regions nearshore shallow waters along the Guangdong

Coastline (regions significantly affected by waves) (Figure 11b). Consequently, the

riverine SSC in summer is was much lower in the downstream of the PRE and in ②-

⑥ regionson the inner shelf east of the Leizhou Peninsula (Figure 9c). This similar

reduction pattern persisted persists in the winter, but is slightly in more western

regions (Figure 9d).

For the NAS case in which ambient shelf currents and residual water levels at the

model boundaries were excluded, the impact on bottom stress is was minimal

compared to the NTS and NWS cases. However, NAS has had a relatively large

impact on the mean circulation (Figures 5a, 6a, and 9e-f). It mainly influences

influenced the summer circulation. Specifically, ignoring these factors would cause

the relatively strong northeastward flow along the Guangdong coast to become very

weak (Figure 9e). When it comes to winter, the influence of NAS on circulation is was

relatively small. That is, in the absence of the background residual water level and

residual circulationcurrent, due to the strong northeastward northeasterly winds in

winter, the overall circulation is was still southwestward (Figure 9f). The

underestimated decreased northeastward flow in summer leads led to the Riverine

SSC being scarcely transported to the vicinity of the "Eastern" and "Southeastern"

regionsEastern Guangdong Coastline. Consequently, the Riverine SSC there is was

decreased (Figure 9e) and sediment deposition is was significantly reduced (Figure

863   11c). Most of the suspended Riverine sediment is ~~was~~ transported southwestward,

864   resulting in an increase in the Riverine SSC along the "Western" region~~Western~~

865   ~~Guangdong Coastline~~. In winter, since most of the suspended Riverine sediment has

866   ~~had~~ been transported southwestward in summer, the Riverine SSC decreases

867   ~~decreased~~ compared to the Control run (Figure 9f). Ultimately, NAS mainly causes

868   ~~caused~~ a significant reduction in sediment deposition in the "Eastern" region~~near the~~

869   ~~Eastern Guangdong Coastline~~, while sediment deposition increases ~~increased~~ in the

870   "Gulf" ~~Beibu Gulf~~ and the "Distal" regions (Figure 11c).

871

872
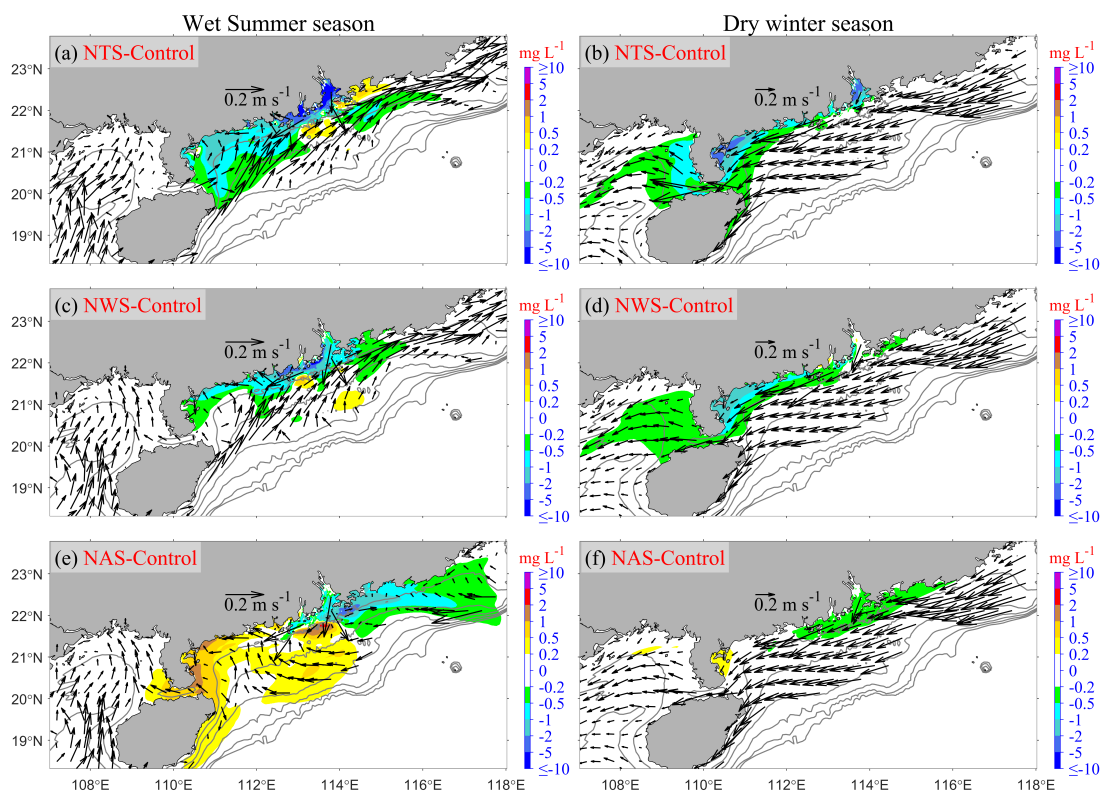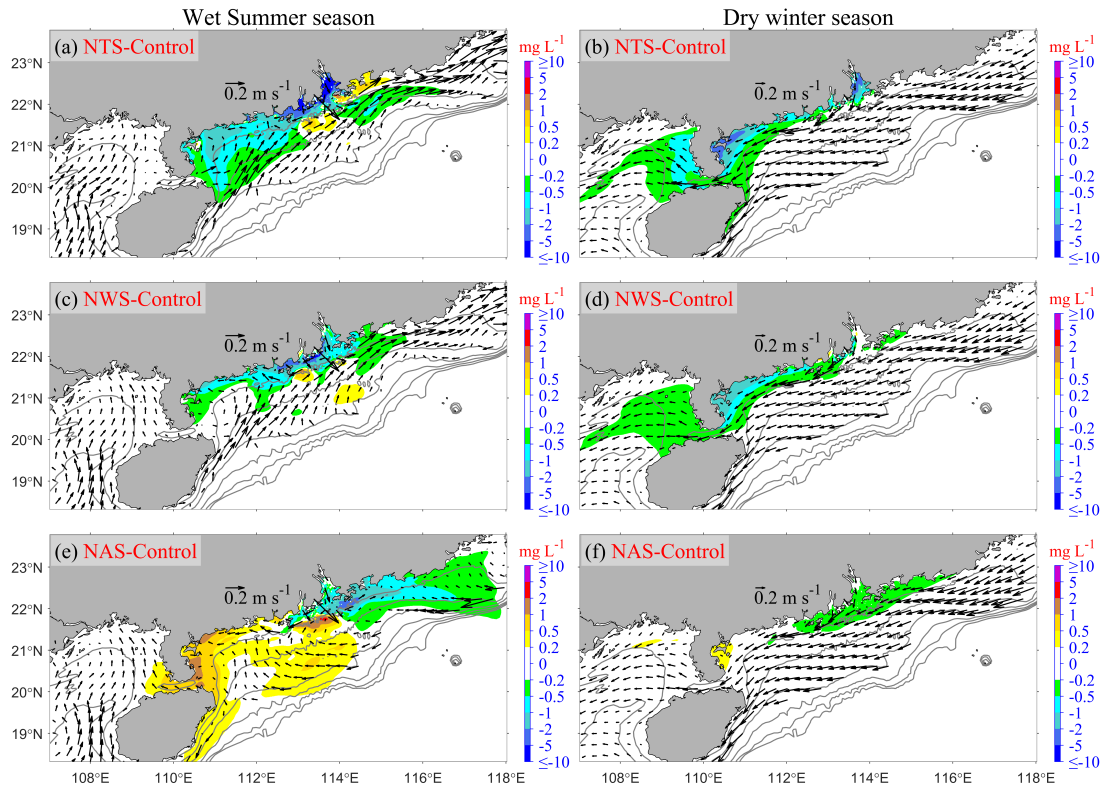
Figure 9. Same as Figure 8, but for seasonal mean differences in surface riverine SSC between the Control run and the following cases: (a-b) NTS-Control, (c-d) NWS-Control, and (e-f) NAS-Control. The first column represents the wet summer season, while the second column corresponds to the dry winter season. Vectors show the seasonal mean surface current fields in each experiment. Note that the riverine SSC values shown in the figure correspond to classes 4 and 5 as defined in Table 1.

For the NVS case, in which the winter and summer critical shear stress for erosion were kept identical, the summer conditions of NVS are were precisely the same as those of the Control run (Figure 10a). Since the critical shear stress for erosion in winter is was lower than that in the Control run, this leads led to an increase

in re-suspension ~~within~~ in the ~~PRE, along the Western Guangdong Coastline,~~ "Proximal", "Western" and ~~in~~ the "Gulf" regions~~Beibu Gulf area~~, increasing ~~resulting in an increase~~ in Riverine SSC (Figure 10b). Eventually, this causes ~~caused~~ a reduction in the deposition thickness of the Pearl River-derived sediments ~~on the continental shelf~~ in these regions(Figure 11d).

In the DSV case~~, where sediment settling velocity was doubled compared to the Control run, riverine SSC patterns remained broadly similar between to~~the ~~two scenarios in both summer and winter. However~~, significant reductions occur ~~occurred~~ in the primarily ~~primarialy~~ high SSC areas in the Control run in both summer and winter~~, with regions of higher SSC in the Control run experiencing the most pronounced declines~~ (Figures 5c, 6c, 10c-d). ~~This~~ The enhanced settling velocity results ~~resulted~~ in an increased deposition of Pearl River-derived sediments along the Guangdong coastline ("Western" and "Eastern" regions) and the eastern "Gulf" region~~Beibu Gulf~~, accompanied by a reduced deposition thickness in the western "Gulf" region ~~Beibu Gulf~~ (Figure 11e).

In the Cycle case, the ~~initial conditions for the five sediment classes were set using the Class 1-5 sediment suspensions and depositions from the Control run on March 31, 2018, initiating a second control simulation.~~ new riverine sediment input and its transport processes during the Cycle experiment are nearly identical to those in the Control run. Therefore, compared to the Control run, the Cycle experiment specifically focuses on examining the impact of the presence of pre-existing Pearl River-derived sediments on estimating the riverine SSC and the annual seabed

riverine sediment budget in the second year. ~~This setup introduced a full year's result~~

~~of Pearl River derived sediment suspensions and depositions into the model domain at~~

~~the start.~~ Consequently, during the ~~initial~~ summer period, the Cycle case experiences

elevated riverine SSC in the primary depocenters identified in the Control run

(Figures 7d and 10e), while this effect is diminished by winter (Figure 10f). ~~This~~

~~experiment specifically examines the impact of pre-existing Pearl River derived~~

~~sediments in the water column and seabed on annual seabed budgets. To isolate this~~

~~effect, the sediment thickness from the Control run's end on March 31, 2018, was~~

~~subtracted as a baseline before comparing annual depositions with the Control run~~

~~(Figure 11f).~~ Figure 11f thus captures the transport trends of pre-existing riverine

sediments in the second year, demonstrating that riverine sediments deposited during

the first year can be resuspended and transported further southwestward during the

second year. This migration is driven by the annually averaged net alongshore coastal

current, which remains predominantly directed toward the southwest. The current

becomes stronger during the winter monsoon under the influence of prevailing

northeasterly winds, whereas the opposing summer southerly winds are comparatively

weaker, indicating a persistent southwestward sediment transport trend over

multi-year timescales.

~~The Cycle case changed the downstream PRE deposition patterns, with increased~~

~~sediment accumulation in downstream regions and notable changes in deposition~~

~~thickness in parts of the Beibu Gulf, revealing a long-term southwestward sediment~~

~~transport trend.~~
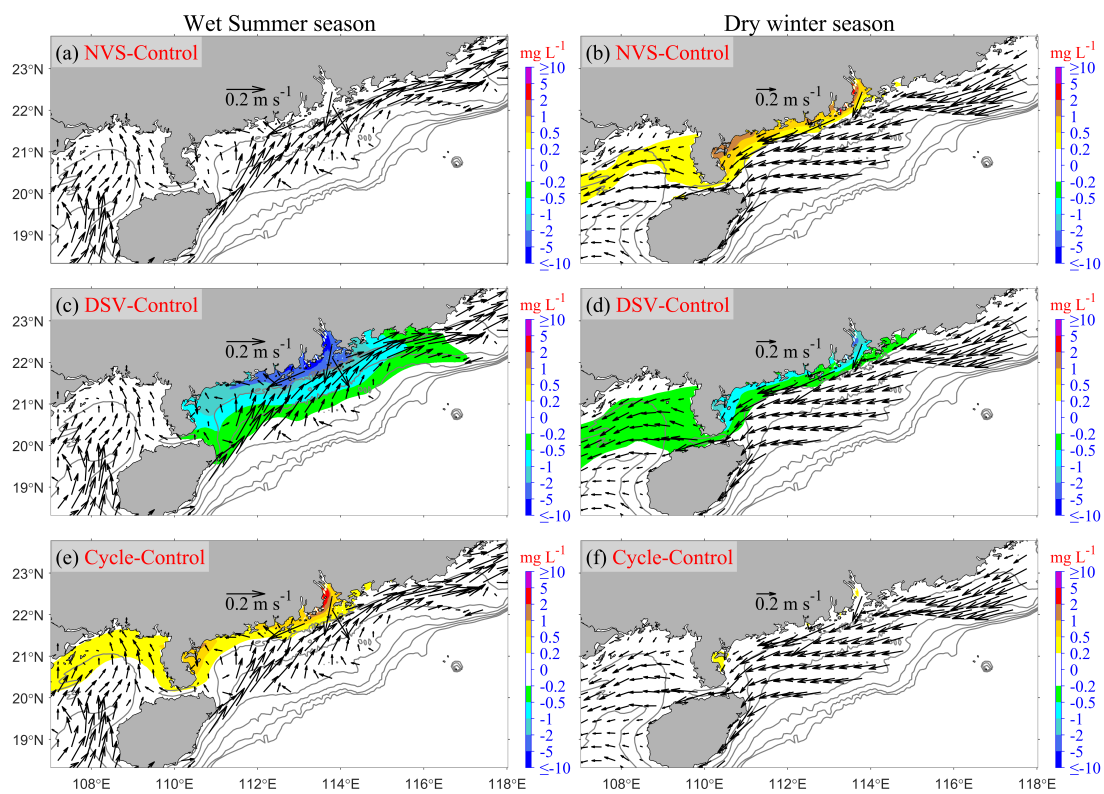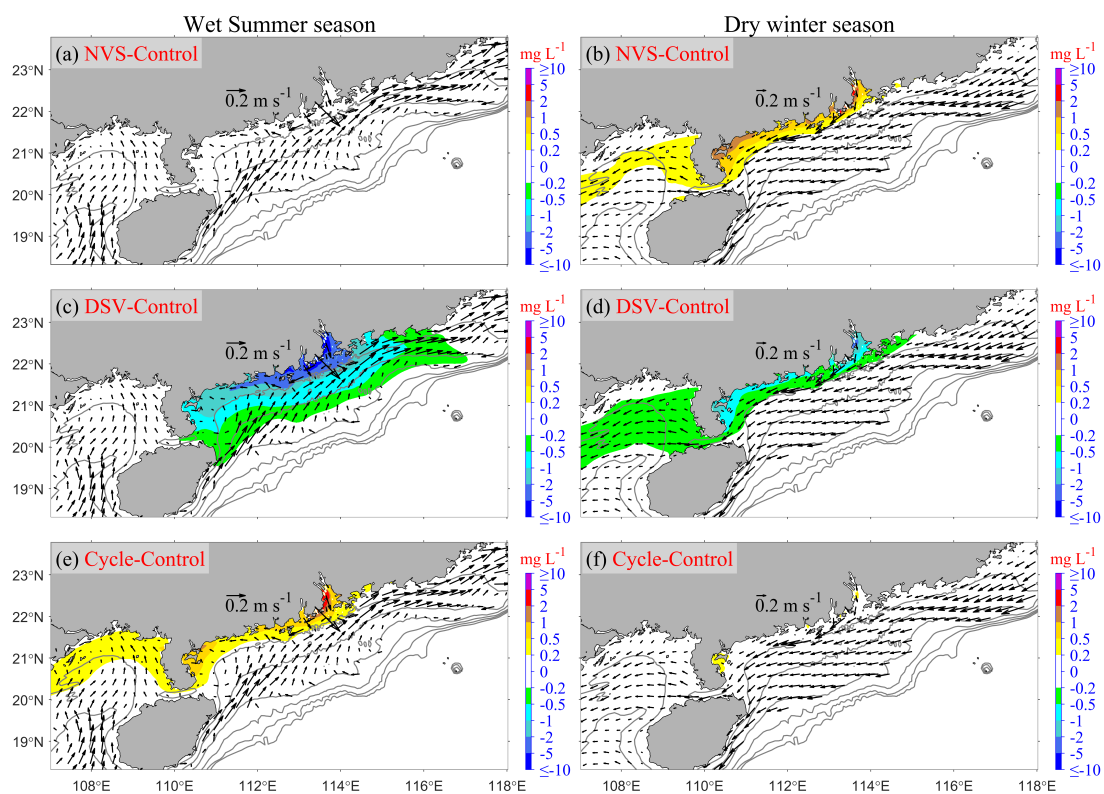
933   **Figure 10.** Same as Figure 9, but for the latter three experiments (NVS, DSV, Cycle).

934   (a-b) NVS-Control, (c-d) DSV-Control, and (e-f) Cycle-Control.

935

936
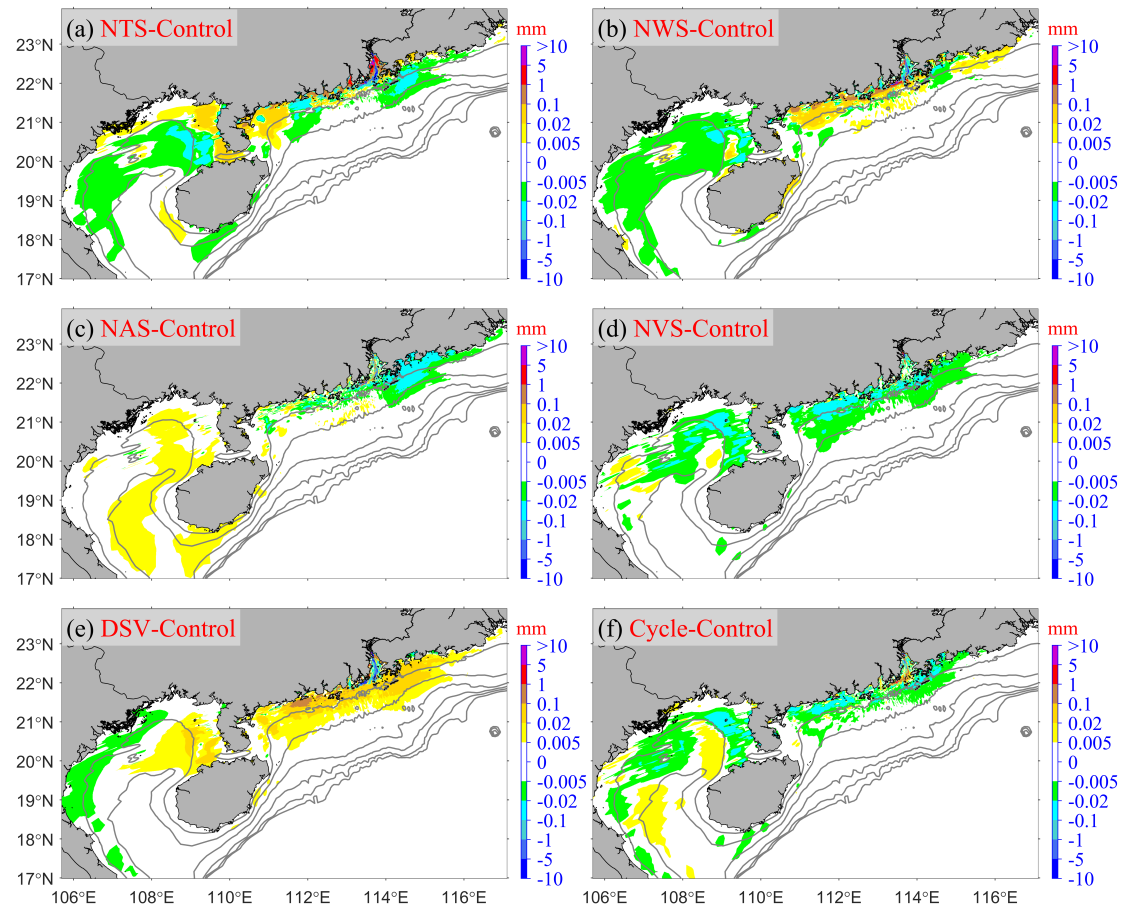
937   **Figure 11.** The differences in annual deposition patterns of Pearl River-derived

938   sediment (classes 4-5, Table 1) on the seabed between the Control run and the

939   following cases: (a) NTS-Control, (b) NWS-Control, (c) NAS-Control, (d)

940   NVS-Control, (e) DSV-Control, and (f) Cycle-Control.

941

942   **3.4 Modeled regional retention budgets in sensitivity experiments**

943   Finally, we analyze the impact of various factors on the annual riverine sediment

944 retention budget across different regions. Specifically, Figure 12 illustrates the annual

945 riverine sediment retention budget in various regions under six sensitivity simulations,

946 namely Exp 2-7 (including NTS, NWS, NAS, NVS, DSV, and Cycle). It should be

947 noted that the retention percentages budget and their variations discussed hereinafter

948 are all relative to the annual riverine sediment load (Figure 3a).

949 As shown in Figure 12, tides and sediment settling velocity have the most

950 significant impact on the retention in the "Proximal" region. In the NTS case and the

951 DSV case, the retention in the "Proximal" region is 70.92% and 71.57%, respectively

952 (Figures 12a and 12e), which is higher than 66.45% in the Control run (Figure 7c).

953 This indicates that ignoring tides will cause the "Proximal" region PRE to capture

954 more riverine sediments, and a larger settling velocity will result in more riverine

955 sediments being retained within the "Proximal" regionPRE. In these two cases,

956 compared with the Control run, the retention in the "Gulf" and "Distal" regions

957 decreases. Meanwhile, the DSV case causes the greatest increase in retention in the

958 "Western" region, with an increase of +1.91%.

959 Furthermore, the NWS also leads to a 2.2% increase in retention in the

960 "Proximal" region (Figure 12b), which is lower than that in the NTS case. This shows

961 that tides dominate resuspension versus deposition in the "Proximal" region estuary

962 more than waves do. However, for the "Western" region on the shelf west of the PRE,

963 compared with the NTS case, the NWS causes a greater increase in retention,

964 indicating that waves dominate the resuspension of Pearl River-derived sediments in

965 these nearshore areas more than tides do.

For ~~the shelf east of the PRE (i.e.,~~ the "Eastern" and "Southeastern" regions~~)~~, NAS brings about the most dramatic changes~~. In the absence of ambient shelf currents and residual water levels~~, the retention of Pearl River-derived sediments in these regions drops from 9.1% to 0.84% compared to the Control run (Figure 12c). Meanwhile, ignoring these background circulations results in a substantial ~~overestimation~~ increase in ~~of~~ the retention in the "Distal" region, with an increase of 6.49%.

~~In t~~The NVS case~~, where the winter and summer critical shear stress for erosion are set to be identical, ignoring the fact that the critical erosion stress in winter should be higher than that in summer~~ leads to a decrease in the retention of the Pearl River-derived sediments in ①−⑥ regions~~on the shelf east of the Leizhou Peninsula and Hainan Island~~ compared to the Control run. The reduction ranges from -0.05% to -0.85% (Figure 12d), which in turn causes the retention in the "Gulf" and "Distal" regions to increase by 0.7% and 1.47%, respectively. Overall, compared with scenarios that ignore physical processes and alter sediment settling velocity (NTS, NWS, NAS, and DSV), the NVS scenario~~, which does not take into account the seasonal variation of critical shear stress for erosion,~~ has a relatively smaller impact on the retention of the Pearl River-derived sediments.

Finally, in the Cycle case, ~~the end state of the Control run is used as the initial conditions, and a second control simulation is performed. To~~ to isolate the pre-existing Pearl River-derived sediments, the initial retentions (the end conditions of the Control run on March 31, 2018) were ~~are~~ subtracted before calculating the retention in the

Cycle case (Figure 12f). ~~In the Cycle case, t~~The retention of Pearl River-derived

sediments in ①–⑥ regions~~on the shelf east of the Leizhou Peninsula and Hainan~~

~~Island~~ shows little variation, with values ranging from -0.98% to +0.24% compared to

the Control run (Figure 12f). The most significant changes are the decreases and

increases in retention in the "Gulf" and "Distal" regions, which are -2.17% and

+3.54%, respectively~~, compared to the Control run~~. This demonstrates the long-term

trend of southwestward transport of Pearl River-derived sediments on the shelf

(relative to the Control run).
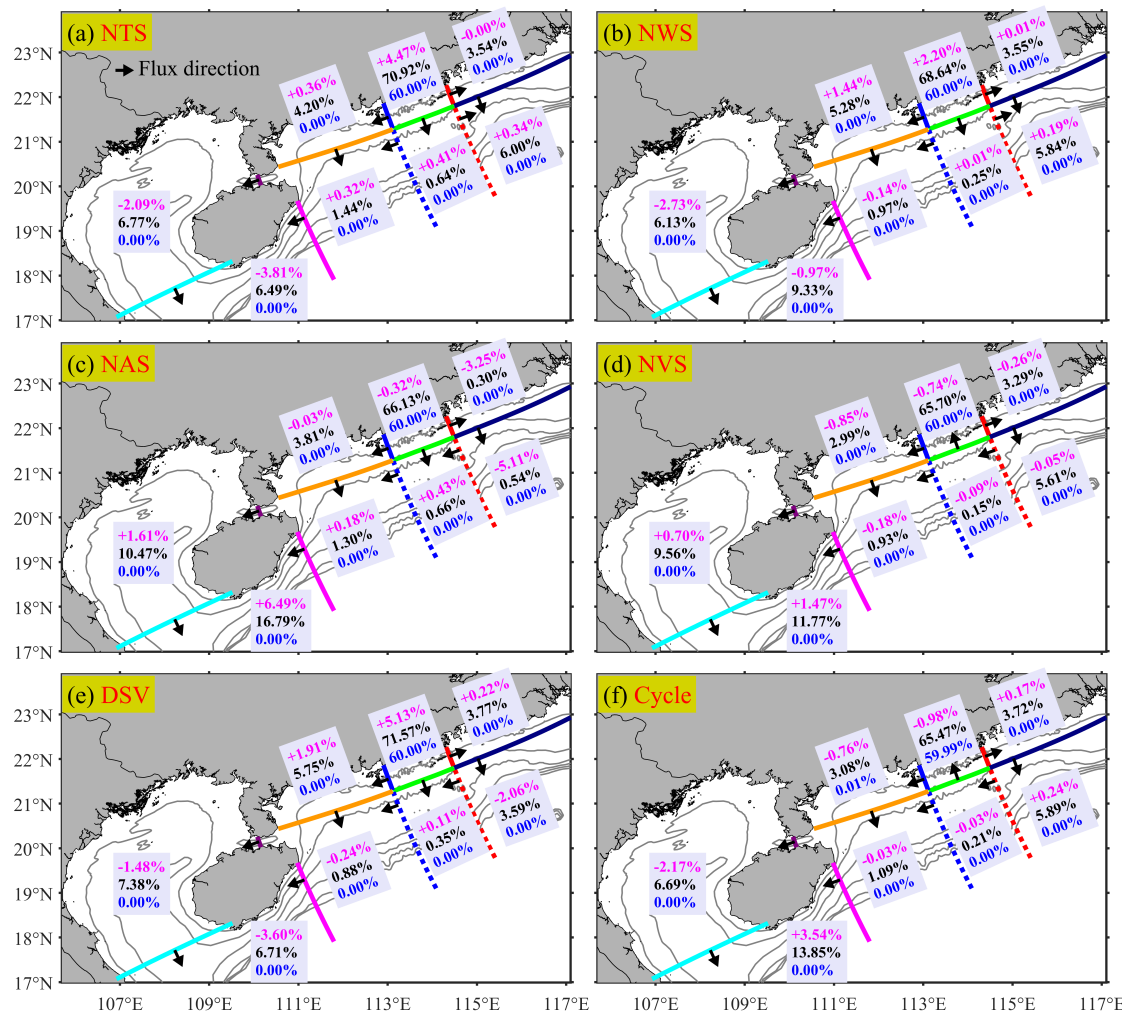
Figure 12. Same as Figure 7c, but for the other six cases: (a) NTS, (b) NWS, (c) NAS, (d) NVS, (e) DSV, and (f) Cycle, respectively. All percentages shown in the figure are expressed relative to the annual riverine sediment load (see Figure. 3a). Magenta values denote the differences in retention percentage of riverine sediments (Classes 4 and 5; Table 1) between the Control run and each sensitivity case. Black values represent the combined retention of Classes 4 + 5, while blue values indicate Class 5 alone. To obtain the retention percentage for Class 4, simply subtract the Class 5 percentage (blue) from the combined Classes 4 + 5 percentage (black).

1007 **Figure 12.** Same as Figure 7c, but for the other six cases: (a) NTS, (b) NWS, (c) NAS,

1008 (d) NVS, (e) DSV, and (f) Cycle, respectively. The magenta percentage values

1009 indicate the retention percentage budget differences between the Control run and the

1010 sensitivity cases.

1011

1012

4. Discussions

4.1 Fidelity of our model results

We simulated the suspension, transport, and deposition of the Pearl River-derived sediment over the shelf from April 2017 to March 2018. Comparisons with multiple types of observations demonstrated that the model simulation reasonably well captured the regional patterns and temporal variability of water levels (Figures S2-S4), surface waves (Figures S5-S6), estuarine and shelf currents (Figures S8a-b and S9-S10), salinity and temperature (Figures S7a-b and S8c-d), and SSC (Figures S7c and S8e-f). Even though we have made substantial efforts to collect observational data and conduct calibration and validation, the large scope of the study area and the fact that the study covers an entire year mean that there are some inherent challenges to achieving a complete analysis. The real-world situation may be extremely complex, and these validations may still not be sufficient to address all issues (such as the accurate parameterization of sediment characteristics and their seasonal variations, as well as the proportion of slow-settling fine grains and flocculated flocs materials in riverine sediments). Therefore, in this section, we intend to discuss the fidelity of our results.

Studies have demonstrated a seasonal dependence of sediment critical shear stress (Xu et al., 2014; Briggs et al., 2015). On the Louisiana shelf, seabed erodibility is controlled by grain size, sediment age, proximity to river sources, bioturbation, and flood deposits, and is higher during the wet season than the dry season (Xu et al., 2014). It is also linked to seasonal hypoxia: sites experiencing hypoxic (hypoxia

greater than 75% of the time, hypoxia defined as < 2 mg O_2 L^{-1}) conditions exhibit

greater erodibility, whereas the normoxic (hypoxia less than 25% of the time) site

shows the lowest erodibility (Briggs et al., 2015). These findings imply that sediment

models should incorporate seasonal variations in critical shear stress, parameterized

using field observations or seasonal sampling data. Similarly, in the PRE, ~~Firstly,~~

field~~according to previous~~ observations, laboratory experiments, and numerical

sensitivity analyses have shown~~, it has been demonstrated~~ that the critical shear stress

for erosion of sediments in the PRE is higher in winter/dry season than in summer/wet

season (Dong et al., 2020; Cao et al., 2025). The summer period in the PRE also

coincides with seasonal hypoxia (Cui et al., 2018; Cui et al., 2022), which likely

contributes to this seasonal variation in erodibility. Therefore, we considered the

seasonal variation of critical shear stress for erosion in a suite of model experiments,

that is, increasing the critical shear stress for erosion in winter. This setting was also

applied during the 15-month spin-up before conducting the model experiments (the

driving force of the spin-up is realistic, i.e., the settings are consistent with those of

the Control run). After realistic reworking during the spin-up, the bed sediment grain

size distribution (used as initial conditions in the Control run and all Sensitivity cases

except the Cycle case) is quite close to the initial prototype (Figures 2d-f vs. 2g-i)

~~compared to our previous spin-up (not presented in this version; however, it can be~~

~~referred to in our initially submitted preprint and Supplement), which did not consider~~

~~such temporal variability~~.

When the seasonal variation of critical shear stress for erosion is omitted (NVS

case)~~not considered~~, the model results suggest ~~of the NVS case indicate that such a~~ ~~setting underestimates the~~ a reduced retention of Pearl River-derived sediments in ① −⑥ regions~~on the shelf east of the Leizhou Peninsula and Hainan Island~~ during winter, alongside an increased~~while overestimating the~~ retention in the "Gulf" and "Distal" regions. However, ~~Even so,~~ these differences ~~estimation errors~~ are relatively small in magnitude ~~minor~~ compared to the annual load (Figure 12d). Thus~~Consequently~~, accounting for~~the consideration of the~~ seasonal variations ~~of~~ in critical shear stress for erosion has a limited ~~relatively small~~ influence ~~impact~~ on the annual-scale retention patterns. ~~Instead, it has a more significant effect on the bed sediment grain size distribution at the bottom.~~

~~Furthermore, although the initial bed sediment grain size distribution we obtained by considering the seasonal variation of critical shear stress for erosion is quite close to the initial prototype, there are still some differences (Figures 2d-f vs. 2g-i). Additionally, the lack of in situ grain size distributions in part of the model domain (especially in the Beibu Gulf) may also introduce some uncertainties in sediment transport there. Does the variation in the proportion of bed sediment grain sizes have a significant impact on the model results? It should be noted that here we are not referring to the distribution proportion of riverine sediments on the bed. To address this question, we designed a new experiment (Cycle2). We used the end state of the Control run on March 31, 2018, as the initial conditions for Cycle2. However, different from the Cycle case, in Cycle2, we changed both Class 1 and Class 4 sediments in the bed and water column at the end state of the Control run to Class 1,~~

and both Class 2 and Class 5 sediments to Class 2. That is, there were no pre-existing Pearl River-derived sediments in the model domain when Cycle2 started. The results of Cycle2 show that the retention in the "Proximal" and "Western" regions decreased by 0.13% and 0.03% of the annual riverine sediment load, respectively, while the retention in the "Eastern", "Southeastern", "Southern", "Southwestern", "Gulf", and "Distal" regions increased by 0.03%, 0.03%, 0.01%, 0.02%, 0.07%, and 0.01%, respectively. This indicates that the impact of this uncertainty in the proportion of bed sediment grain sizes is relatively small.

The dispersal distance of fluvial sediments on continental shelves is strongly influenced by settling velocity (Harris et al., 2008). For example, Apennine-derived sediments, characterized by lower settling velocities, travel farther before deposition than Po River sediments, which are predominantly flocculated and settle more rapidly (Fox et al., 2004; Harris et al., 2008). Likewise, our results suggest that selecting Choosing an appropriate settling velocity parameter exerts a greater control on sediment dispersal patternsmay be more important than accounting for the seasonal variations of in critical shear stress for erosion (Figure 12d vs. 12e). The results of the DSV case show that a sediment settling velocity twice that of the Control run leads to the highest retention in the "Proximal" and "Western" regions across all experiments (Figure 12e), while reducing the retention in the "Distal" region (Figure 12e). Although the settling velocity we adopted is based on previous studies (Xia et al., 2004) and model calibrations (Figures S7c and S8e-f), with due consideration given to the presence of slow-settling single fine grains and high-settling flocs in riverine

1101 sediments, certain discrepancies might still exist in this setting. These discrepancies

1102 are contingent upon the actual magnitude of the low settling velocity of fine grains. In

1103 almost all cases, all flocs are retained in the "Proximal" region (Figure 12a-e), and

1104 only in the Cycle case, flocs accounting for 0.01% of the annual load are retained in

1105 the "Western" region west of the "Proximal" region (Figure 12f, blue values),

1106 indicating that high-settling flocs hardly leave the "Proximal" region~~vicinity of the~~

1107 ~~PRE~~. This finding shows close alignment with, yet exhibits minor distinctions from,

1108 the observed patterns in the Mekong ~~Estuary~~ Shelf (Xue et al., 2012). Xue et al. (2012)

1109 found that while the preponderance of flocs is deposited on the Mekong delta front

1110 precisely at the river mouth, a quantity equivalent to 1.6% of the annual riverine

1111 sediment load of flocs is deposited on the downdrift delta front further downstream

1112 from the river mouth. This is mainly because the estuarine ~~estuary~~ bay of the PRE is

1113 wider and there are numerous islands near the river mouth. The overwhelming

1114 majority of flocs are either deposited within the estuarine bay or captured by the

1115 surrounding islands. In conclusion, our results are affected by the settling velocity of

1116 fine grains. More field observations and studies on model parameterization regarding

1117 the settling velocity of fine grains are urgently needed.

1118   As previously noted, we classified riverine sediments into two categories based

1119 on established research: 40% slow-settling fine grains and 60% fast-settling flocs.

1120 This 40%/60% distribution is consistent with the setting from earlier studies (Zhang et

1121 al., 2019; Zhang et al., 2021), as summarized in Table 1. While such assumptions are

1122 necessary for modeling purposes, the actual composition of riverine sediments in

1123   natural environments remains uncertain. To evaluate the sensitivity of our results to

1124   this uncertainty, we conducted a conceptual analysis. If all riverine sediments were

1125   hypothetically composed entirely of fast-settling flocs, they would be completely

1126   retained near the source, with no transport to the "Gulf" region~~Beibu Gulf~~. However,

1127   this scenario is inconsistent with the radionuclide measurements obtained from "Gulf"

1128   region~~Beibu Gulf~~ surface sediment samples (Lin et al., 2020). On the other hand, if all

1129   sediments were considered slow-settling fine grains, only 16.13% would be retained

1130   in "Proximal" region ~~proximally~~ under normal conditions (or 28.9% in the DSV case),

1131   a result that diverges significantly from established research. Chen et al. (2023)

1132   analyzed high-resolution seismic data and demonstrated that approximately 35% of

1133   the Pearl River-derived sediment has been transported to offshore shelf areas over the

1134   past 6,500 years, suggesting that 65% was deposited proximally. Our findings are in

1135   close agreement, indicating that 66.45% of the Pearl River sediments are retained in

1136   the proximal region, while 33.55% are transported elsewhere. This consistency with

1137   Chen et al. (2023) supports the validity of our approach. Taken together, these

1138   analyses confirm that the 40%/60% fraction assumption is a reasonable approximation

1139   for modeling purposes.

1140   Furthermore, our model results demonstrate reasonable reliability in other aspects.

1141   Liu et al. (2009) and Ge et al. (2014) using chirp sonar profiles from the inner shelf of

1142   the South China Sea combined with Zong et al. (2009)'s onshore borehole data, found

1143   that the thickness of Pearl River-derived sediments within the PRE since the Holocene

1144   is over 20 m, while the mud thickness in the shallow waters west of the Chuanshan

Islands (see Figure 1) is approximately 5-10 m. Our calculated annual sediment thicknesses for these two regions are approximately 2 mm and 0.3 mm (Figure 7d), respectively. Given our model's annual riverine sediment load of 34.52 megatons, which has been —significantly reduced due to recent human activities (Dai et al., 2008), —compared to the widely accepted Holocene average of around 90 megatons (Liu et al., 2009), we estimate the total sediment thickness over the past 7500 years to be roughly 39 meters and 6 meters for these depositional zones, consistent with previous studies (Liu et al., 2009; Zong et al., 2009).

Furthermore, our results reveal that 8.86% of the riverine sediment derived from the Pearl River is transported to the "Gulf" region Beibu Gulf (Figure 7c), primarily during the winter season (Figure 7b). This finding is not only consistent with confirms the earlier speculation proposed by Ge et al. (2014) but also supplements the conclusions drawn by Lin et al. (2020). From a hydrodynamic perspective, Shi et al. (2002) found that the net flux of currents in the Qiongzhou Strait is westward throughout the year. Our results for both wet summer (Figures 5a-b) and dry winter currents (Figures 6a-b) in the Qiongzhou Strait are consistent with Shi et al. (2002). This westward flow contributes to the westward transport of Pearl River sediment to the "Gulf" region Beibu Gulf.

4.2 Implications of our model results

The fate of sediment dispersed from the river into the coastal ocean involves at least four processes: supply via buoyant plumes; initial deposition; resuspension and

1167   transport by marine processes; and long-term net accumulation (Wright and Nittrouer,

1168   1995). In general, a significant proportion of river sediment tends to deposit in the

1169   estuary and its vicinity (Walsh and Nittrouer, 2009; Hanebuth et al., 2015).

1170   Walsh and Nittrouer (2009) present a hierarchical decision tree designed to

1171   predict the marine dispersal system at a river mouth based on fundamental

1172   oceanographic and morphological characteristics. Within this framework, ~~the fate of~~

1173   riverine sediment deposition is characterized~~can be determined~~ using key factors,

1174   including –riverine sediment discharge (greater or less than 2 megatons), shelf width

1175   (greater or less than 12 km), and wave and tidal range conditions (greater or less than

1176   2 m) (Walsh and Nittrouer, 2009).

1177   We aim to analyze our PRE simulation results using the framework established

1178   by Walsh and Nittrouer (2009). Although the Pearl River's riverine sediment

1179   discharge (Figure 2a) exceeds the Walsh and Nittrouer (2009)'s 2 megatons per year

1180   threshold, most of the sediment still remains deposited near the estuary (Figure 7c),

1181   indicating an estuarine accumulation-dominated (EAD) system, unlike the

1182   hierarchical decision tree proposed by Walsh and Nittrouer (2009). Outside the estuary,

1183   the continental shelf, spanning 200-220 km in width (Liu et al., 2014), significantly

1184   exceeds –Walsh and Nittrouer (2009)'s 12 km threshold. As a result, most escaped

1185   riverine sediments tend to accumulate on the shelf rather than being captured by

1186   submarine canyons (Figures 7c-d). This wide, shallow shelf promotes sediment

1187   deposition and limits the direct transport of fine sediments into deeper waters (Walsh

1188   and Nittrouer, 2009). Subsequently, given that the annual mean tidal range (Chen et

1189 al., 2016; Gong et al., 2018b) and Hsig (Figure 3d) near the PRE are both below the 2

1190 m threshold established by Walsh and Nittrouer (2009), the majority of escaped

1191 riverine sediments are predominantly deposited in the proximal depo-center. Our

1192 findings demonstrate that most of our outcomes are consistent with the hierarchical

1193 decision tree proposed by Walsh and Nittrouer (2009), except for the application of

1194 the 2 megatons per year threshold for riverine sediment discharge. This phenomenon

1195 can primarily be attributed to the unique geomorphological characteristics of the PRE,

1196 including its broad mouth (Figures 1 and S1), extensive accommodation space

1197 encompassing approximately 2385 km^2 of water area (Wu et al., 2018), the presence

1198 and sheltering effect of numerous adjacent islands (Li et al., 2024b), and the division

1199 of fluvial sediment discharge through eight distinct outlets (Hu et al., 2011).

1200 The monsoonal nature of the northern SCS (Figures 4a-b) induces pronounced

1201 seasonal variations in Pearl River-derived sediment transport and deposition (Figures

1202 5 and 6). During the summer wet season, the Pearl River delivers approximately 95.17%

1203 of its annual sediment load to the PRE and the adjacent shelf (Figure 7a) under

1204 relatively calm wind and wave conditions (first column of Figure 4), leading to

1205 predominant proximal deposition (Figure 5f). In contrast, the winter dry season is

1206 characterized by strong northeasterly monsoon winds that generate high-energy waves

1207 (second column of Figure 4), significantly increasing bottom shear stress (Figures

1208 4g-h). This process resuspends previously deposited sediments and facilitates their

1209 redistribution, particularly toward regions such as the "Gulf" region~~Beibu Gulf~~

1210 (Figure 6f).

The PRE exhibits distinctive geomorphological features, yet dispersal of its fine-grained sediment transport on the continental shelf conforms to general patterns observed offshore of ~~in~~ other monsoon-influenced estuarine systems. Similar multiple-stage sediment delivery and dispersal mechanisms have been documented offshore of ~~in~~ various major estuaries and their adjacent shelves, including the Yellow River Shelf ~~Estuary~~ (Bian et al., 2013; Zeng et al., 2015), Changjiang River Shelf ~~Estuary~~ (Zeng et al., 2015), and Mekong River Shelf ~~Estuary~~ (Xue et al., 2012; Eidam et al., 2017), demonstrating comparable sedimentary processes under monsoon climatic influences. In these systems, sediment transport is not confined to a single process but rather occurs in stages, influenced by seasonal variations in hydrodynamic conditions. Like the PRE Shelf, the Mekong Shelf experiences distinct phases of sediment deposition, with fine sediments being delivered during periods of high river discharge and then redistributed by waves and tidal forces, particularly during monsoonal shifts (Xue et al., 2012; Eidam et al., 2017). These complex patterns highlight the interplay between riverine inputs, coastal morphology, and oceanographic processes in shaping sediment dynamics.

These sediment delivery patterns have implications beyond sediment fate, particularly for carbon cycling. Sediment deposition in coastal and shelf areas plays a significant role in trapping organic carbon, influencing long-term carbon burial rates (LaRowe et al., 2020). Sediment dynamics directly influence the fate of organic carbon (OC) in marine environments, where sediments function as both a sink and a source of OC, playing a pivotal role in global carbon cycling (Repasch et al., 2021).

1233 The multiple-step transport mechanisms can lead to varying carbon storage locations,

1234 affecting the sequestration potential of these systems. Additionally, resuspension and

1235 redistribution of sediments, especially during high-energy events, may expose

1236 previously buried organic material, leading to carbon remineralization and influencing

1237 coastal nutrient cycles and ecosystem health (Ståhlberg et al., 2006; Moriarty et al.,

1238 2018). Therefore, understanding these patterns is crucial for assessing the broader

1239 impacts on carbon cycling and coastal biogeochemical processes.

1240 ~~Furthermore, we evaluated the contributions of different physical processes by~~

1241 ~~comparing the Control run with sensitivity cases. Our analysis reveals distinct roles of~~

1242 ~~tidal forces, wave action, and background circulation in governing the transport and~~

1243 ~~deposition of Pearl River-derived sediments (Figures 8, 9, 11a-c, and 12a-c).~~

1244 ~~Tidal dynamics predominantly influence sediment behavior within the PRE.~~

1245 ~~Neglecting tidal effects leads to an underestimation of bottom shear stress within the~~

1246 ~~estuary (Figures 8a-b), resulting in an overestimation of sediment deposition (Figure~~

1247 ~~11a) and consequently underestimating distal sediment retention (Figure 12a).~~

1248 ~~Wave activity primarily controls sediment resuspension in three critical~~

1249 ~~dimensions: (1) the river mouth, (2) the eastern and western nearshore regions outside~~

1250 ~~the estuary, and (3) periods characterized by high wave energy during winter (Figures~~

1251 ~~9c-d). The exclusion of wave effects results in overestimated sediment deposition in~~

1252 ~~these areas and periods (Figure 11b), ultimately leading to an underestimation of~~

1253 ~~sediment accumulation thickness in the Beibu Gulf (Figure 11b).~~

1254 ~~Background circulation exerts its most significant influence during the summer~~

months (Figure 5a vs. Figure 9e). The strong northeastward background current in summer serves as the primary driver for transporting Pearl River-derived sediments to the continental shelf east of the PRE. When considering only the weak southerly winds without the northeastward background current, merely 0.84% of Pearl River sediments are transported to the eastern shelf, substantially overestimating distal deposition (Figure 12c).

4.3 Limitations and future work Future Work

This study focuses on analyzing simulation results from a typical year, encompassing both wet and dry seasons from 2017 to 2018, to understand the seasonal variations and annual patterns of suspension, transport, and deposition of sediment in the PRE and adjacent shelf. However, it's essential to recognize that the long-term sediment transport and deposition dynamics in the Pearl River are influenced by numerous complex factors. These include changes in sea level and coastal line (Church and White, 2006; Harff et al., 2010; Hong et al., 2020; Lin et al., 2022; Ma et al., 2023), alterations in wind field and precipitation (Ning and Qian, 2009; Young et al., 2011), natural sedimentation within the Pearl River Delta (Wu et al., 2010), modifications in sediment load and underwater volume of the estuary caused by anthropogenic impact (Wu et al., 2014; Wu et al., 2018; Lin et al., 2022), interannual variations of the shelf circulations (Liu et al., 2020; Deng et al., 2022) and Kuroshio intrusions (Caruso et al., 2006; Nan et al., 2015; Sun et al., 2020). Therefore, while this study sheds light on seasonal and annual timescale patterns, it cannot fully represent the short or long-term transport and deposition trends of the Pearl River

sediment. Yet for many shelf systems, a lot of ~~the~~ sediment transport happens during short-lived events such as hurricanes (Xu et al., 2016; Warner et al., 2017; Georgiou et al., 2024). Consideration of the episodicity of transport would be helpful for future studies (Xu et al., 2016; Warner et al., 2017; Georgiou et al., 2024).

Additionally, it's important to note that this article primarily focuses on the fate of the Pearl River sediment on the inner shelf. ~~However, there are other smaller rivers within the Pearl River plume's expansion range, like the Han River, Rong River, Moyang River, Jian River, and Nandu River (Liu et al., 2016).~~ However, within the expansion range of the Pearl River buoyant plume, a number of smaller rivers, including the Jiulong River, Han River, Moyang River, Jian River, Nanliu River, Changhua River and Nandu River, also contribute freshwater and sediment to the northern South China Sea (Milliman and Farnsworth, 2011; Zhang et al., 2012; Liu et al., 2016). Although these rivers contribute significantly less freshwater and sediment compared to the Pearl River, they still impact seawater salinity, suspended sediment concentration, and seabed geomorphology (Liu et al., 2016; Wang et al., 2023; Zong et al., 2024). Since the 1950s, South China delivers approximately 102 Mt/year of fluvial sediment to the SCS, with the Pearl River alone accounting for 84.3 Mt/year—about 83% of the total sediment load (Milliman and Farnsworth, 2011; Zhang et al., 2012; Liu et al., 2016). The specific contributions of each river are detailed in Table 3. While the data highlight the Pearl River's dominant role in sediment delivery, a comprehensive understanding of sedimentary processes and impacts in the northern South China Sea also requires systematic investigation into

the roles of the smaller contributing rivers.

Table 3. Annual mean runoff and annual suspended sediment load of major rivers in South China that flow directly into the northern South China Sea since the 1950s (Milliman and Farnsworth, 2011; Zhang et al., 2012; Liu et al., 2016).

River name	Runoff ($m^3 s^{-1}$)	Suspended sediment load (Mt/year)
Pearl River	9075	84.3
Jiulong River	476	3.1
Han River	825	10
Moyang River	269	0.8
Jian River	174	1.5
Nanliu River	162	1.1
Changhua River	120	0.08
Nandu River	179	0.4

~~Hence, there is a need for further systematic research to understand the processes and impacts of these smaller rivers comprehensively.~~

~~Lastly~~Then, while the model used in this study has shown good validation results, conducting more sensitivity experiments on sediment parameters, such as settling velocity and critical shear stress for erosion, would be beneficial. Settling velocity can influence the location of sediment depocenters, with higher settling velocities leading to more proximal entrapment and vice versa (Harris et al., 2008) ~~(Ralston and Geyer, 2017)~~. Similarly, critical erosion stress can affect the resuspension of deposited

1312 sediment, with higher critical erosion stress resulting in less resuspension and more

1313 deposition especially during neap tides and weak wind wave events (Dong et al., 2020;

1314 Choi et al., 2023). Conducting such sensitivity analyses would enhance our

1315 understanding of sediment dynamics in estuaries and shelves. Besides, the model does

1316 not account for cohesive processes, such as consolidation and flocculation, which can

1317 significantly impact sediment behavior (Sherwood et al., 2018). Our model does not

1318 incorporate wave and current-supported gravity flows, which are important factors

1319 influencing sediment transport in submarine canyon areas (Harris et al., 2005; Ma et

1320 al., 2010; Zhang et al., 2020). Since our study area primarily focuses on the

1321 continental shelf and the simulated results indicate that sediment transport occurs

1322 mainly in the shallow inner shelf, where canyons are relatively rare, this omission has

1323 a relatively minor impact on our results.

1324 Lastly, we employ the COAWST model, which uses an S-coordinate system in

1325 the vertical direction with increased resolution near the surface and bottom layers

1326 (Song and Haidvogel, 1994). This vertical layering allows cell heights to vary,

1327 enabling finer resolution in dynamically important regions and improving

1328 performance in areas with sloping bathymetry compared to traditional

1329 sigma-coordinate systems (Bryan, 1969; Song and Haidvogel, 1994). In addition, our

1330 model includes horizontal grid refinement in the PRE, enhancing its ability to resolve

1331 estuarine features. As a result, the model effectively captures estuarine turbidity

1332 maxima (ETM) and horizontal salinity fronts (Figures S11 and S12, see Supplement).

1333 During summer, multiple ETMs appear near the estuary bottom (Figure S11b), and

while these features persist in winter, their concentrations vary (Figure S12b), consistent with the findings of Wang et al. (2018), Zhan et al. (2019), Zhang et al. (2021), Ma et al. (2022), and Ma et al. (2024). Horizontal salinity fronts are also well represented, showing an upstream shift from the high-discharge summer season to the low-discharge winter season (Figures S11e–f and S12e–f), in agreement with previous studies by Zhang et al. (2021) and Ma et al. (2024). Nonetheless, compared with the S-coordinate system, models that employ vertically adaptive layering (e.g., SCHISM, the Semi-implicit Cross-scale Hydroscience Integrated System Model, Zhang et al. (2016)) or Cartesian vertical coordinates (e.g., MITgcm, the MIT General Circulation Model, Marshall et al. (1997a); Marshall et al. (1997b)) generally perform better in regions with steep topographic gradients (Bijvelds, 2001). Therefore, future research could benefit from adopting models with higher horizontal resolution and Cartesian vertical coordinates to improve the simulation of Pearl River-derived sediment dynamics across the estuary and the adjacent shelf.

5. Conclusions

This study utilizes the COAWST model to quantitatively analyze the seasonal suspension, transport, and annual fate of Pearl River-derived sediment (classes 4-5 in Table 1) on the continental shelf over a typical year, capturing key marine variables such as water level, wave height, flow velocity, salinity, temperature, and SSC.

The monsoonal nature of the northern SCS (Figures 4a-b) induces pronounced seasonal variations in Pearl River-derived sediment transport and deposition (Figures

5 and 6). During the wet summer, calm conditions foster initial Pearl River-derived sediment deposition via the buoyant ~~river~~ plume (Figures 5 and 7a). Conversely, winter's stronger winds and waves resuspend and transport Pearl River-derived sediments into "Gulf" region~~Beibu Gulf, primarily during this dry season~~ (Figures 6 and 7b). Our quantitative assessment reveals distinct spatial patterns in the annual fate of riverine sediments: approximately two-thirds~~66.45%~~ of the Pearl River-derived ~~total~~ sediment ~~load~~ is retained within the estuarine vicinity ("Proximal" region), while about 9%~~9.2%~~ reaches~~is deposited on~~ the continental shelf east of the PRE ("Eastern" and "Southeastern" regions), while similar proportions are ~~. Furthermore, 8.86% and 10.3% of the sediment is~~ transported to and retained in "Gulf" and "Distal" regions~~the Beibu Gulf and the area south of Hainan Island~~, respectively (Figure 7c).

Furthermore, we evaluated the contributions of different physical processes by comparing the Control run with the reduced-physics sensitivity experiments. Our analysis reveals distinct roles of tidal forces, wave action, and background circulation in governing the transport and deposition of Pearl River-derived sediments (Figures 8, 9, 11a-c, and 12a-c).

Tidal dynamics primarily govern sediment behavior within and offshore of ~~in~~ the PRE. Relative to the Control run, ~~Neglecting~~ neglecting tides leads to lower ~~underestimates the~~ bottom shear stress in the PRE (Figures 8a-b), higher ~~overestimates~~ Pearl River-derived sediment deposition in the PRE (Figure 11a), and reduced ~~underestimates distal~~ sediment retention in "Gulf" and "Distal" regions (Figure 12a). Wave activity primarily controls Pearl River-derived sediment

resuspension in three critical dimensions: (1) the river mouth, (2) the nearshore of "Eastern" ~~eastern~~ and "Western" ~~western nearshore~~ regions outside the estuary, and (3) periods characterized by high wave energy during winter (Figures 9c-d). Excluding waves results in increased~~leads to overestimated~~ modeled Pearl River-derived sediment deposition in these areas and times (Figure 11b), while reducing ~~underestimating~~ accumulation in the "Gulf" region~~Beibu Gulf~~ (Figure 11b). Background circulation is most influential in summer (Figure 5a vs. Figure 9e), with a strong northeastward current transporting Pearl River-derived sediments to regions ③−④~~the eastern shelf~~. Without this current and under weak southerly winds, only 0.84% of Pearl River-derived sediments are transported to ~~reach the~~ regions ③−④ ~~eastern shelf~~, while deposition in ~~overestimating~~ "Gulf" and "Distal" regions ~~distal deposition~~ is greater compared to the Control run (Figure 12c). The sediment model solutions are also highly sensitive to the parameterization of sediment characteristics and spin-up durations (riverine or seabed sediments) ~~initial conditions~~ (Figures 10, 11d-f, and 12d-f). Neglecting the seasonal increase in~~need for a higher~~ critical shear stress for erosion leads to enhanced~~in winter overestimates~~ resuspension and erosion in regions ①−⑥~~on the shelf east of the Leizhou Peninsula~~ during winter~~this season~~ (Figure 10b), which in turn shifts more sediment toward "Gulf" and "Distal" regions compared to the Control run ~~leading to a greater distal retention~~ (Figure 12d). Increasing the settling velocity reduces the overall riverine SSC (Figures 10c-d) and results in a spatial redistribution pattern characterized by greater retention in ①−③ and ⑤ regions and reduced riverine sediment presence in "Gulf" and "Distal"

regions relative to the Control simulation~~while overestimating the proximal retention and underestimating the distal retention~~ (Figure 12e). Additionally, the model~~ed~~ riverine SSC ~~solutions are~~is influenced by pre-existing Pearl River–derived sediments, as shown in the Cycle experiment (Figure 10e-f)~~ initial conditions~~. The experiment highlights the effect of riverine sediment spin-up, showing that first-year retained Pearl River–derived sediments are predominantly redistributed from the "Gulf" region toward the more distant "Distal" region during the second year.~~If the model domain initially includes a full year of Pearl River-derived sediment retention, re-running the simulation results in further transport of previously retained sediments from the Beibu Gulf to more distal areas.~~ In contrast~~However~~, the model exhibits only minor sensitivity~~is relatively insensitive~~ to the duration of seabed sediment spin-up, as demonstrated in the Cycle2 experiment~~the initial bed grain size distribution~~ (~~Experiment Cycle2;~~ see Supplement~~Section 4.1~~), in which riverine sediments present during the spin-up period were added to seabed sediment classes 1–2 at the start of the Cycle2.

Acknowledgments

This research was funded by the National Natural Science Foundation of China (grant numbers 42306015 and 42276169), the China Postdoctoral Science Foundation (grant number 2023M743988). Wenping Gong is supported by the Southern Marine Science and Engineering Guangdong Laboratory (Zhuhai) (SML2023SP238). The authors would like to thank the crew of the R/V Changhe Ocean for their valuable

1422 contribution during the collection of the field- data. We express our gratitude to the

1423 Co-editors-in-chief, Dr. Mario Hoppema, and three two anonymous reviewers for

1424 their valuable suggestions in enhancing and improving this article.

Data availability

1426   The HYbrid Coordinate Ocean Model (HYCOM) outputs are from:

1427 http://hycom.org/hycom. The NCEP Climate Forecast System Version 2 (CFSv2)

1428 reanalysis data can be obtained at the following website:

1429 https://rda.ucar.edu/datasets/ds094.1/dataaccess/. The NOAA WAVEWATCH III

1430 global ocean wave model output fields can be downloaded from:

1431 ftp://polar.ncep.noaa.gov/pub/history/waves. Hourly water-level data observed at

1432 Quarry Bay station are provided by the Hong Kong Observatory website:

1433 https://www.hko.gov.hk/sc/tide/marine/realtide.htm?s=QUB&t=TABLE. Hourly

1434 water-level data from Zhapo and Qinglan stations, provided by the Flanders Marine

1435 Institute (VLIZ), are part of the UNESCO/IOC Global Sea Level Observing System

1436 (GLOSS) and accessible at http://www.ioc-sealevelmonitoring.org. The mooring data

1437 for the M1 and M2 stations are sourced from Liu et al. (2023) and Li et al. (2024a).

1438 The figure data and model configuration files used in this paper can be downloaded

1439 from: https://doi.org/10.5281/zenodo.15013448.

Declaration of Competing interests

1441   The authors declare that they have no known competing financial interests or

1442 personal relationships that could have appeared to influence the work reported in this

1443 paper.

CRediT authorship contribution statement

~~Guang Zhang~~GZ: Conceptualization, Numerical modeling, Validation, Data visualization, Writing-original draft, and Funding acquisition. ~~Suan Hu~~SH: Writing-review & editing, Validation. ~~Xiaolong Yu~~XY: Writing-review & editing. ~~Heng Zhang~~HZ: Writing-review & editing. ~~Wenping Gong~~WG: Writing-review & editing, and Funding acquisition

Supplement:

The Supplement ~~We have included~~ includes ~~the~~ validation~~s~~ and analysis of the model's water levels, Hsig, flow velocities, salinity, temperature, and SSC ~~in the Supplement~~. It provides additional text and figures that support the model validation and supplementary analyses, which could not be fully presented in the main article due to space limitations.

References

Bever, A. J., Harris, C. K., Sherwood, C. R., and Signell, R. P.: Deposition and flux of sediment from the Po River, Italy: An idealized and wintertime numerical modeling study, Marine Geology, 260, 69-80, 10.1016/j.margeo.2009.01.007, 2009.

Bever, A. J., and MacWilliams, M. L.: Simulating sediment transport processes in San Pablo Bay using coupled hydrodynamic, wave, and sediment transport models, Marine Geology, 345, 235-253, 10.1016/j.margeo.2013.06.012, 2013.

Bian, C., Jiang, W., and Greatbatch, R. J.: An exploratory model study of sediment transport sources and deposits in the Bohai Sea, Yellow Sea, and East China Sea, Journal of Geophysical Research: Oceans, 118, 5908-5923, https://doi.org/10.1002/2013JC009116, 2013.

Bijvelds, M. D. J. P.: Numerical modelling of estuarine flow over steep topography, Doctoral, Delft University of Technology, 2001.

Booij, N., Ris, R. C., and Holthuijsen, L. H.: A third-generation wave model for coastal regions: 1.

1469 Model description and validation, Journal of Geophysical Research: Oceans, 104, 7649-7666,

1470 https://doi.org/10.1029/98JC02622, 1999.

1471 Brand, A., Lacy, J. R., Hsu, K., Hoover, D., Gladding, S., and Stacey, M. T.: Wind-enhanced

1472 resuspension in the shallow waters of South San Francisco Bay: Mechanisms and potential

1473 implications for cohesive sediment transport, Journal of Geophysical Research, 115,

1474 10.1029/2010jc006172, 2010.

1475 Briggs, K. B., Cartwright, G., Friedrichs, C. T., and Shivarudruppa, S.: Biogenic effects on cohesive

1476 sediment erodibility resulting from recurring seasonal hypoxia on the Louisiana shelf, Continental

1477 Shelf Research, 93, 17-26, https://doi.org/10.1016/j.csr.2014.11.005, 2015.

1478 Bryan, K.: A numerical method for the study of the circulation of the world ocean, Journal of

1479 Computational Physics, 4, 347-376, https://doi.org/10.1016/0021-9991(69)90004-7, 1969.

1480 Burchard, H., Schuttelaars, H. M., and Ralston, D. K.: Sediment Trapping in Estuaries, Annual Review

1481 of Marine Science, 10, 371-395, 10.1146/annurev-marine-010816-060535, 2018.

1482 Cao, L., Liu, J., Shi, X., He, W., and Chen, Z.: Source-to-sink processes of fluvial sediments in the

1483 northern South China Sea: Constraints from river sediments in the coastal region of South China,

1484 Journal of Asian Earth Sciences, 185, 104020, 10.1016/j.jseaes.2019.104020, 2019.

1485 Cao, Z., Ren, J., Deng, Z., Ye, L., and Wu, J.: Small-scale spatial variability in erosion threshold and

1486 bedform for cohesive sediment measured by 3D Sonar, Journal of Hydrology, 650, 132513,

1487 10.1016/j.jhydrol.2024.132513, 2025.

1488 Caruso, M. J., Gawarkiewicz, G. G., and Beardsley, R. C.: Interannual variability of the Kuroshio

1489 intrusion in the South China Sea, Journal of Oceanography, 62, 559-575,

1490 10.1007/s10872-006-0076-0, 2006.

1491 Chapman, D. C.: Numerical Treatment of Cross-Shelf Open Boundaries in a Barotropic Coastal Ocean

1492 Model, Journal of Physical Oceanography, 15, 1060-1075, 1985.

1493 Charnock, H.: Wind stress on a water surface, Quarterly Journal of the Royal Meteorological Society,

1494 81, 639-640, https://doi.org/10.1002/qj.49708135027, 1955.

1495 Chassignet, E. P., Hurlburt, H. E., Smedstad, O. M., Halliwell, G. R., Hogan, P. J., Wallcraft, A. J.,

1496 Baraille, R., and Bleck, R.: The HYCOM (HYbrid Coordinate Ocean Model) data assimilative

1497 system, Journal of Marine Systems, 65, 60-83, https://doi.org/10.1016/j.jmarsys.2005.09.016,

2007.

Chen, S.-N., Geyer, W. R., Sherwood, C. R., and Ralston, D. K.: Sediment transport and deposition on a river-dominated tidal flat: An idealized model study, Journal of Geophysical Research, 115, 10.1029/2010jc006248, 2010.

Chen, Y., Deng, B., Saito, Y., Wang, Z., Yang, X., and Wu, J.: Pearl River sediment dispersal over its associated delta–estuary–shelf system during the Holocene, Sedimentology, 70, 2331-2354, 10.1111/sed.13123, 2023.

Chen, Z., Pan, J., and Jiang, Y.: Role of pulsed winds on detachment of low salinity water from the Pearl River Plume Upwelling and mixing processes, Journal of Geophysical Research: Oceans, 121, 2769-2788, 10.1002/2015JC011337, 2016.

Chen, Z., Gong, W., Cai, H., Chen, Y., and Zhang, H.: Dispersal of the Pearl River plume over continental shelf in summer, Estuarine, Coastal and Shelf Science, 194, 252-262, 10.1016/j.ecss.2017.06.025, 2017a.

Chen, Z., Pan, J., Jiang, Y., and Lin, H.: Far-reaching transport of Pearl River plume water by upwelling jet in the northeastern South China Sea, Journal of Marine Systems, 173, 60-69, 10.1016/j.jmarsys.2017.04.008, 2017b.

Cheng, P., Li, M., and Li, Y.: Generation of an estuarine sediment plume by a tropical storm, Journal of Geophysical Research: Oceans, 118, 856-868, 10.1002/jgrc.20070, 2013.

Choi, S. M., Seo, J. Y., and Ha, H. K.: Contribution of local erosion enhanced by winds to sediment transport in intertidal flat, Marine Geology, 465, 107171, 10.1016/j.margeo.2023.107171, 2023.

Church, J. A., and White, N. J.: A 20th century acceleration in global sea-level rise, Geophysical Research Letters, 33, n/a-n/a, 10.1029/2005gl024826, 2006.

Cui, Y., Wu, J., Ren, J., and Xu, J.: Physical dynamics structures and oxygen budget of summer hypoxia in the Pearl River Estuary, Limnology and Oceanography, 64, 131-148, 10.1002/lno.11025, 2018.

Cui, Y., Wu, J., Tan, E., and Kao, S. J.: Role of Particle Resuspension in Maintaining Hypoxic Level in the Pearl River Estuary, Journal of Geophysical Research: Oceans, 127, 10.1029/2021jc018166, 2022.

Dai, S. B., Yang, S. L., and Cai, A. M.: Impacts of dams on the sediment flux of the Pearl River,

1527   southern China, Catena, 76, 36-43, 10.1016/j.catena.2008.08.004, 2008.

1528   Dalyander, P. S., Butman, B., Sherwood, C. R., Signell, R. P., and Wilkin, J. L.: Characterizing wave-

1529   and current- induced bottom shear stress: U.S. middle Atlantic continental shelf, Continental Shelf

1530   Research, 52, 73-86, https://doi.org/10.1016/j.csr.2012.10.012, 2013.

1531   Deng, Y., Liu, Z., Zu, T., Hu, J., Gan, J., Lin, Y., Li, Z., Quan, Q., and Cai, Z.: Climatic Controls on the

1532   Interannual Variability of Shelf Circulation in the Northern South China Sea, Journal of

1533   Geophysical Research: Oceans, 127, e2022JC018419, https://doi.org/10.1029/2022JC018419,

1534   2022.

1535   Dong, H., Jia, L., He, Z., Yu, M., and Shi, Y.: Application of parameters and paradigms of the erosion

1536   and deposition for cohesive sediment transport modelling in the Lingdingyang Estuary, China,

1537   Applied Ocean Research, 94, 101999, 10.1016/j.apor.2019.101999, 2020.

1538   Dong, L., Su, J., Wong, L., Cao, Z., and Chen, J.: Seasonal variation and dynamics of the Pearl River

1539   plume, Continental Shelf Research, 24, 1761-1777, 10.1016/j.csr.2004.06.006, 2004.

1540   Egbert, G. D., and Erofeeva, S. Y.: Efficient inverse Modeling of barotropic ocean tides, Journal of

1541   Atmospheric and Oceanic Technology, 19, 183-204, Doi

1542   10.1175/1520-0426(2002)019<0183:Eimobo>2.0.Co;2, 2002.

1543   Eidam, E. F., Nittrouer, C. A., Ogston, A. S., DeMaster, D. J., Liu, J. P., Nguyen, T. T., and Nguyen, T.

1544   N.: Dynamic controls on shallow clinoform geometry: Mekong Delta, Vietnam, Continental Shelf

1545   Research, 147, 165-181, 10.1016/j.csr.2017.06.001, 2017.

1546   Fairall, C. W., Bradley, E. F., Rogers, D. P., Edson, J. B., and Young, G. S.: Bulk parameterization of

1547   air-sea fluxes for Tropical Ocean-Global Atmosphere Coupled-Ocean Atmosphere Response

1548   Experiment, Journal of Geophysical Research: Oceans, 101, 3747-3764,

1549   https://doi.org/10.1029/95JC03205, 1996.

1550   Flather, R. A.: A tidal model of the north-west European continental shelf, Memoires Societe Royale

1551   des Sciences de Liege, 10, 141-164, 1976.

1552   Fox, J. M., Hill, P. S., Milligan, T. G., Ogston, A. S., and Boldrin, A.: Floc fraction in the waters of the

1553   Po River prodelta, Continental Shelf Research, 24, 1699-1715,

1554   https://doi.org/10.1016/j.csr.2004.05.009, 2004.

1555   Gan, J., Cheung, A., Guo, X., and Li, L.: Intensified upwelling over a widened shelf in the northeastern

1556    South China Sea, Journal of Geophysical Research, 114, 10.1029/2007jc004660, 2009.

1557  Gan, J., San Ho, H., and Liang, L.: Dynamics of Intensified Downwelling Circulation over a Widened

1558    Shelf in the Northeastern South China Sea, Journal of Physical Oceanography, 43, 80-94,

1559    10.1175/jpo-d-12-02.1, 2013.

1560  Gao, S., and Collins, M. B.: Holocene sedimentary systems on continental shelves, Marine Geology,

1561    352, 268-294, 10.1016/j.margeo.2014.03.021, 2014.

1562  Gao, X., Chen, S., Xie, X., Long, A., and Ma, F.: Non-aromatic hydrocarbons in surface sediments near

1563    the Pearl River estuary in the South China Sea, Environmental Pollution, 148, 40-47,

1564    10.1016/j.envpol.2006.11.001, 2007.

1565  Gao, X., Arthur Chen, C.-T., Wang, G., Xue, Q., Tang, C., and Chen, S.: Environmental status of Daya

1566    Bay surface sediments inferred from a sequential extraction technique, Estuarine, Coastal and

1567    Shelf Science, 86, 369-378, 10.1016/j.ecss.2009.10.012, 2010.

1568  Ge, Q., Liu, J. P., Xue, Z., and Chu, F.: Dispersal of the Zhujiang River (Pearl River) derived sediment

1569    in the Holocene, Acta Oceanologica Sinica, 33, 1-9, 10.1007/s13131-014-0407-8, 2014.

1570  Ge, Q., Xue, Z., Yao, Z., Zang, Z., and Chu, F.: Anti-phase relationship between the East Asian winter

1571    monsoon and summer monsoon during the Holocene?, Journal of Ocean University of China, 16,

1572    175-183, 10.1007/s11802-017-3098-x, 2017.

1573  Ge, Q., Xu, D., Ye, L., Yang, K., and Yao, Z.: Linking Monsoon Activity with River-Derived Sediments

1574    Deposition in the Northern South China Sea, Journal of Ocean University of China, 18, 1098-1104,

1575    10.1007/s11802-019-4155-4, 2019.

1576  Georgiou, I. Y., FitzGerald, D. M., Sakib, M. M., Messina, F., Kulp, M. A., and Miner, M. D.: Storm

1577    Dynamics Control Sedimentation and Shelf-Bay-Marsh Sediment Exchange Along the Louisiana

1578    Coast,   Geophysical   Research   Letters,   51,   e2024GL111344,

1579    https://doi.org/10.1029/2024GL111344, 2024.

1580  Geyer, W. R., Hill, P. S., and Kineke, G. C.: The transport, transformation and dispersal of sediment by

1581    buoyant coastal flows, Continental Shelf Research, 24, 927-949, 10.1016/j.csr.2004.02.006, 2004.

1582  Gong, W., Chen, Y., Zhang, H., and Chen, Z.: Effects of Wave–Current Interaction on Salt Intrusion

1583    During a Typhoon Event in a Highly Stratified Estuary, Estuaries and Coasts, 41, 1904-1923,

1584    10.1007/s12237-018-0393-8, 2018a.

1585   Gong, W., Lin, Z., Chen, Y., Chen, Z., Shen, J., and Zhang, H.: Effect of waves on the dispersal of the
1586   Pearl River plume in winter, Journal of Marine Systems, 186, 47-67,
1587   10.1016/j.jmarsys.2018.05.003, 2018b.

1588   Haidvogel, D. B., Arango, H., Budgell, W. P., Cornuelle, B. D., Curchitser, E., Di, L. E., Fennel, K.,
1589   Geyer, W. R., Hermann, A. J., Lanerolle, L., Levin, J., McWilliams, J. C., Miller, A. J., Moore, A.
1590   M., Powell, T. M., Shchepetkin, A. F., Sherwood, C. R., Signell, R. P., Warner, J. C., and Wilkin, J.:
1591   Ocean forecasting in terrain-following coordinates: Formulation and skill assessment of the
1592   Regional Ocean Modeling System, Journal of Computational Physics, 227, 3595-3624,
1593   10.1016/j.jcp.2007.06.016, 2008.

1594   Hanebuth, T. J. J., Lantzsch, H., and Nizou, J.: Mud depocenters on continental shelves—appearance,
1595   initiation times, and growth dynamics, Geo-Marine Letters, 35, 487-503,
1596   10.1007/s00367-015-0422-6, 2015.

1597   Harff, J., Leipe, T., and Zhou, D.: Pearl River Estuary related sediments as response to Holocene
1598   climate change and anthropogenic impact (PECAI), Journal of Marine Systems, 82, S1-S2,
1599   10.1016/j.jmarsys.2010.02.008, 2010.

1600   Harris, C. K., Traykovski, P. A., and Geyer, W. R.: Flood dispersal and deposition by near-bed
1601   gravitational sediment flows and oceanographic transport: A numerical modeling study of the Eel
1602   River shelf, northern California, Journal of Geophysical Research: Oceans, 110,
1603   10.1029/2004jc002727, 2005.

1604   Harris, C. K., Sherwood, C. R., Signell, R. P., Bever, A. J., and Warner, J. C.: Sediment dispersal in the
1605   northwestern Adriatic Sea, Journal of Geophysical Research, 113, 10.1029/2006jc003868, 2008.

1606   Hong, B., Liu, Z., Shen, J., Wu, H., Gong, W., Xu, H., and Wang, D.: Potential physical impacts of
1607   sea-level rise on the Pearl River Estuary, China, Journal of Marine Systems, 201, 103245,
1608   10.1016/j.jmarsys.2019.103245, 2020.

1609   Hu, J., Li, S., and Geng, B.: Modeling the mass flux budgets of water and suspended sediments for the
1610   river network and estuary in the Pearl River Delta, China, Journal of Marine Systems, 88, 252-266,
1611   10.1016/j.jmarsys.2011.05.002, 2011.

1612   Hu, S., Li, Y., Hu, P., Zhang, H., Zhang, G., and Gong, W.: The Impacts of Far-Field Typhoon-
1613   Generated Coastal Trapped Waves on the Hydrodynamics in the Northern South China Sea: A

1614   Case Study of Typhoon In - Fa, Journal of Geophysical Research: Oceans, 129,

1615   10.1029/2024jc021359, 2024.

1616   Huang, D., Du, J., Deng, B., and Zhang, J.: Distribution patterns of particle-reactive radionuclides in

1617   sediments off eastern Hainan Island, China: Implications for source and transport pathways,

1618   Continental Shelf Research, 57, 10-17, 10.1016/j.csr.2012.04.019, 2013.

1619   Jacob, R., Larson, J., and Ong, E.: M × N Communication and Parallel Interpolation in Community

1620   Climate System Model Version 3 Using the Model Coupling Toolkit, IJHPCA, 19, 293-307,

1621   10.1177/1094342005056116, 2005.

1622   Kirby, M. F., Devoy, B., Law, R. J., Ward, A., and Aldridge, J.: The use of a bioassay based approach to

1623   the hazard/risk assessment of cargo derived toxicity during shipping accidents: a case study--the

1624   MSC Napoli, Marine Pollution Bulletin, 56, 781-786, 10.1016/j.marpolbul.2008.01.006, 2008.

1625   Krige, D. G.: A Statistical Approach to Some Basic Mine Valuation Problems on the Witwatersrand,

1626   Chemical, Metallurgical and Mining Society of South Africa, 1951.

1627   Kuehl, S. A., Alexander, C. R., Blair, N. E., Harris, C. K., Marsaglia, K. M., Ogston, A. S., Orpin, A. R.,

1628   Roering, J. J., Bever, A. J., Bilderback, E. L., Carter, L., Cerovski-Darriau, C., Childress, L. B.,

1629   Reide Corbett, D., Hale, R. P., Leithold, E. L., Litchfield, N., Moriarty, J. M., Page, M. J., Pierce,

1630   L. E. R., Upton, P., and Walsh, J. P.: A source-to-sink perspective of the Waipaoa River margin,

1631   Earth-Science Reviews, 153, 301-334, 10.1016/j.earscirev.2015.10.001, 2016.

1632   Kumar, N., Voulgaris, G., Warner, J. C., and Olabarrieta, M.: Implementation of the vortex force

1633   formalism in the coupled ocean-atmosphere-wave-sediment transport (COAWST) modeling

1634   system for inner shelf and surf zone applications, Ocean Modelling, 47, 65-95,

1635   10.1016/j.ocemod.2012.01.003, 2012.

1636   LaRowe, D. E., Arndt, S., Bradley, J. A., Estes, E. R., Hoarfrost, A., Lang, S. Q., Lloyd, K. G.,

1637   Mahmoudi, N., Orsi, W. D., Shah Walter, S. R., Steen, A. D., and Zhao, R.: The fate of organic

1638   carbon in marine sediments - New insights from recent data and analysis, Earth-Science Reviews,

1639   204, 103146, 10.1016/j.earscirev.2020.103146, 2020.

1640   Larson, J., Jacob, R., and Ong, E.: The Model Coupling Toolkit: A New Fortran90 Toolkit for Building

1641   Multiphysics Parallel Coupled Models, IJHPCA, 19, 277-292, 2005.

1642   Li, J., Li, M., and Xie, L.: Observations of near-inertial oscillations trapped at inclined front on

continental shelf of the northwestern South China Sea, EGUsphere, 2024, 1-25, 10.5194/egusphere-2024-3909, 2024a.

Li, X., Chrysagi, E., Klingbeil, K., and Burchard, H.: Impact of Islands on Tidally Dominated River Plumes: A High-Resolution Modeling Study, Journal of Geophysical Research: Oceans, 129, e2023JC020272, https://doi.org/10.1029/2023JC020272, 2024b.

Lin, S., Niu, J., Liu, G., Wei, X., and Cai, S.: Variations of suspended sediment transport caused by changes in shoreline and bathymetry in the Zhujiang (Pearl) River Estuary in the wet season, Acta Oceanologica Sinica, 41, 54-73, 10.1007/s13131-022-2017-1, 2022.

Lin, W., Feng, Y., Yu, K., Lan, W., Wang, Y., Mo, Z., Ning, Q., Feng, L., He, X., and Huang, Y.: Long-lived radionuclides in marine sediments from the Beibu Gulf, South China Sea: Spatial distribution, controlling factors, and proxy for transport pathway, Marine Geology, 424, 106157, 10.1016/j.margeo.2020.106157, 2020.

Liu, G., and Cai, S.: Modeling of suspended sediment by coupled wave-current model in the Zhujiang (Pearl) River Estuary, Acta Oceanologica Sinica, 38, 22-35, 10.1007/s13131-019-1455-3, 2019.

Liu, H., Ye, L., Zhou, W., and Wu, J.: Salt-wedge intrusion-retreat cycle induced sediment floc dynamics in bottom boundary layer (BBL) of a micro-tidal estuary, Marine Geology, 466, 107175, 10.1016/j.margeo.2023.107175, 2023.

Liu, J. P., Xue, Z., Ross, K., Yang, Z., and Gao, S.: Fate of Sediments Delivered to the Sea by Asian Large Rivers: Long-Distance Transport and Formation of Remote Alongshore Clinothems, Sediment. Rec., 7, 10.2110/sedred.2009.4.4, 2009.

Liu, N., Geng, B., Xue, H., Xiu, P., Wang, Q., and Wang, D.: Interannual Variability of Shelf and Slope Circulations in the Northern South China Sea, Journal of Ocean University of China, 19, 1005-1016, 10.1007/s11802-020-4446-9, 2020.

Liu, Y., Gao, S., Wang, Y. P., Yang, Y., Long, J., Zhang, Y., and Wu, X.: Distal mud deposits associated with the Pearl River over the northwestern continental shelf of the South China Sea, Marine Geology, 347, 43-57, 10.1016/j.margeo.2013.10.012, 2014.

Liu, Z., Zhao, Y., Colin, C., Stattegger, K., Wiesner, M. G., Huh, C.-A., Zhang, Y., Li, X., Sompongchaiyakul, P., You, C.-F., Huang, C.-Y., Liu, J. T., Siringan, F. P., Le, K. P., Sathiamurthy, E., Hantoro, W. S., Liu, J., Tuo, S., Zhao, S., Zhou, S., He, Z., Wang, Y., Bunsomboonsakul, S.,

1672   and Li, Y.: Source-to-sink transport processes of fluvial sediments in the South China Sea,

1673   Earth-Science Reviews, 153, 238-273, 10.1016/j.earscirev.2015.08.005, 2016.

1674   Lu, X., Wang, Z., Guo, X., Gu, Y., Liang, W., and Liu, L.: Impacts of metal contamination and

1675   eutrophication on dinoflagellate cyst assemblages along the Guangdong coast of southern China,

1676   Marine Pollution Bulletin, 120, 239-249, 10.1016/j.marpolbul.2017.05.032, 2017.

1677   Ma, C., Zhao, J., Ai, B., Sun, S., and Yang, Z.: Machine Learning Based Long-Term Water Quality in

1678   the Turbid Pearl River Estuary, China, Journal of Geophysical Research: Oceans, 127,

1679   10.1029/2021jc018017, 2022.

1680   Ma, M., Zhang, W., Chen, W., Deng, J., and Schrum, C.: Impacts of morphological change and

1681   sea-level rise on stratification in the Pearl River Estuary, Frontiers in Marine Science, Volume 10 -

1682   2023, 10.3389/fmars.2023.1072080, 2023.

1683   Ma, M., Porz, L., Schrum, C., and Zhang, W.: Physical mechanisms, dynamics and interconnections of

1684   multiple estuarine turbidity maximum in the Pearl River estuary, Frontiers in Marine Science,

1685   Volume 11 - 2024, 10.3389/fmars.2024.1385382, 2024.

1686   Ma, Y., Friedrichs, C. T., Harris, C. K., and Wright, L. D.: Deposition by seasonal wave- and

1687   current-supported sediment gravity flows interacting with spatially varying bathymetry: Waiapu

1688   shelf, New Zealand, Marine Geology, 275, 199-211, https://doi.org/10.1016/j.margeo.2010.06.001,

1689   2010.

1690   Madsen, O. S.: Spectral Wave-Current Bottom Boundary Layer Flows, Coastal Engineering 1, 384-398,

1691   1994.

1692   Mao, Q., Shi, P., Yin, K., Gan, J., and Qi, Y.: Tides and tidal currents in the Pearl River Estuary,

1693   Continental Shelf Research, 24, 1797-1808, 10.1016/j.csr.2004.06.008, 2004.

1694   Marshall, J., Adcroft, A., Hill, C., Perelman, L., and Heisey, C.: A finite-volume, incompressible Navier

1695   Stokes model for studies of the ocean on parallel computers, Journal of Geophysical Research:

1696   Oceans, 102, 5753-5766, https://doi.org/10.1029/96JC02775, 1997a.

1697   Marshall, J., Hill, C., Perelman, L., and Adcroft, A.: Hydrostatic, quasi-hydrostatic, and nonhydrostatic

1698   ocean modeling, Journal of Geophysical Research: Oceans, 102, 5733-5752,

1699   https://doi.org/10.1029/96JC02776, 1997b.

1700   McKee, B. A., Aller, R. C., Allison, M. A., Bianchi, T. S., and Kineke, G. C.: Transport and

1701   transformation of dissolved and particulate materials on continental margins influenced by major

1702   rivers: benthic boundary layer and seabed processes, Continental Shelf Research, 24, 899-926,

1703   https://doi.org/10.1016/j.csr.2004.02.009, 2004.

1704 McWilliams, J. C., Restrepo, J. M., and Lane, E. M.: An asymptotic theory for the interaction of waves

1705   and currents in coastal waters, Journal of Fluid Mechanics, 511, 135-178,

1706   10.1017/s0022112004009358, 2004.

1707 Meade, R. H.: Landward Transport of Bottom Sediments in Estuaries of the Atlantic Coastal Plain,

1708   Journal of Sedimentary Petrology, 39, 222-234, 1969.

1709 Milliman, J., and Farnsworth, K. L.: River discharge to the coastal ocean: A global synthesis. UK:

1710   Cambridge University Press; ISBN 978-0-521-87987-3, 2011.

1711 Moriarty, J. M., Harris, C. K., Friedrichs, M. A. M., Fennel, K., and Xu, K.: Impact of Seabed

1712   Resuspension on Oxygen and Nitrogen Dynamics in the Northern Gulf of Mexico: A Numerical

1713   Modeling Study, Journal of Geophysical Research: Oceans, 123, 7237-7263,

1714   https://doi.org/10.1029/2018JC013950, 2018.

1715 Nan, F., Xue, H., and Yu, F.: Kuroshio intrusion into the South China Sea: A review, Progress in

1716   Oceanography, 137, 314-333, https://doi.org/10.1016/j.pocean.2014.05.012, 2015.

1717 Ning, L., and Qian, Y.: Interdecadal change in extreme precipitation over South China and its

1718   mechanism, Advances in Atmospheric Sciences, 26, 109-118, 10.1007/s00376-009-0109-x, 2009.

1719 Nittrouer, C. A., and Wright, L. D.: Transport of particles across continental shelves, Reviews of

1720   Geophysics, 32, 85-113, https://doi.org/10.1029/93RG02603, 1994.

1721 Orlanski, I.: A simple boundary condition for unbounded hyperbolic flows, Journal of Computational

1722   Physics, 21, 251-269, 10.1016/0021-9991(76)90023-1, 1976.

1723 Ou, S., Zhang, H., and Wang, D.: Dynamics of the buoyant plume off the Pearl River Estuary in

1724   summer, Environmental Fluid Mechanics, 9, 471-492, 10.1007/s10652-009-9146-3, 2009.

1725 Ralston, D. K., Geyer, W. R., and Warner, J. C.: Bathymetric controls on sediment transport in the

1726   Hudson River estuary: Lateral asymmetry and frontal trapping, Journal of Geophysical Research:

1727   Oceans, 117, 10.1029/2012jc008124, 2012.

1728 Ralston, D. K., and Geyer, W. R.: Sediment Transport Time Scales and Trapping Efficiency in a Tidal

1729   River, Journal of Geophysical Research: Earth Surface, 122, 2042-2063, 10.1002/2017jf004337,

2017.

Raymond, W. H., and Kuo, H. L.: A radiation boundary condition for multi-dimensional flows, Quarterly Journal of the Royal Meteorological Society, 110, 535-551, 1984.

Repasch, M., Scheingross, J. S., Hovius, N., Lupker, M., Wittmann, H., Haghipour, N., Gröcke, D. R., Orfeo, O., Eglinton, T. I., and Sachse, D.: Fluvial organic carbon cycling regulated by sediment transit time and mineral protection, Nature Geoscience, 14, 842-848, 10.1038/s41561-021-00845-7, 2021.

Saha, S., Moorthi, S., Wu, X., Wang, J., Nadiga, S., Tripp, P., Behringer, D., Hou, Y.-T., Chuang, H.-y., Iredell, M., Ek, M., Meng, J., Yang, R., Mendez, M. P., van den Dool, H., Zhang, Q., Wang, W., Chen, M., and Becker, E.: The NCEP Climate Forecast System Version 2, Journal of Climate, 27, 2185-2208, https://doi.org/10.1175/JCLI-D-12-00823.1, 2014.

Sanford, L. P.: Wave-forced resuspension of upper Chesapeake Bay muds, Estuaries, 17, 148-165, 1994.

Shchepetkin, A. F., and McWilliams, J. C.: The regional oceanic modeling system (ROMS): a split-explicit, free-surface, topography-following-coordinate oceanic model, Ocean Modelling, 9, 347-404, https://doi.org/10.1016/j.ocemod.2004.08.002, 2005.

Shepard, F. P.: Nomenclature Based on Sand-silt-clay Ratios, Journal of Sedimentary Research, 24, 151-158, 1954.

Sherwood, C. R., Aretxabaleta, A. L., Harris, C. K., Rinehimer, J. P., Verney, R., and Ferré, B.: Cohesive and mixed sediment in the Regional Ocean Modeling System (ROMS v3.6) implemented in the Coupled Ocean–Atmosphere–Wave–Sediment Transport Modeling System (COAWST r1234), Geoscientific Model Development, 11, 1849-1871, 10.5194/gmd-11-1849-2018, 2018.

Shi, M., Chen, C., Xu, Q., Lin, H., Liu, G., Wang, H., Wang, F., and Yan, J.: The Role of Qiongzhou Strait in the Seasonal Variation of the South China Sea Circulation, Journal of Physical Oceanography, 32, 103-121, 2002.

Skamarock, W. C., Klemp, J. B., Dudhia, J., Gill, D. O., Barker, D. M., Wang, W., and Powers, J. G.: A Description of the Advanced Research WRF Version 2, 2005,

Smagorinsky, J.: GENERAL CIRCULATION EXPERIMENTS WITH THE PRIMITIVE

1759   EQUATIONS, Monthly Weather Review, 91, 99-164,

1760   10.1175/1520-0493(1963)091<0099:gcewtp>2.3.co;2, 1963.

1761 Song, Y., and Haidvogel, D.: A Semi-implicit Ocean Circulation Model Using a Generalized

1762   Topography-Following Coordinate System, Journal of Computational Physics, 115, 228-244,

1763   https://doi.org/10.1006/jcph.1994.1189, 1994.

1764 Ståhlberg, C., Bastviken, D., Svensson, B. H., and Rahm, L.: Mineralisation of organic matter in

1765   coastal sediments at different frequency and duration of resuspension, Estuarine, Coastal and Shelf

1766   Science, 70, 317-325, https://doi.org/10.1016/j.ecss.2006.06.022, 2006.

1767 Su, J.: Overview of the South China Sea circulation and its influence on the coastal physical

1768   oceanography outside the Pearl River Estuary, Continental Shelf Research, 24, 1745-1760,

1769   10.1016/j.csr.2004.06.005, 2004.

1770 Sun, Z., Zhang, Z., Qiu, B., Zhang, X., Zhou, C., Huang, X., Zhao, W., and Tian, J.: Three-Dimensional

1771   Structure and Interannual Variability of the Kuroshio Loop Current in the Northeastern South

1772   China Sea, Journal of Physical Oceanography, 50, 2437-2455,

1773   https://doi.org/10.1175/JPO-D-20-0058.1, 2020.

1774 Tolman, H., Accensi, M., Alves, J.-H., Ardhuin, F., Barbariol, F., Benetazzo, A., Bennis, A.-C., Bidlot,

1775   J., Booij, N., Boutin, G., Campbell, T., Chalikov, D., Chawla, A., Cheng, S., Collins Iii, C., Filipot,

1776   J.-F., Foreman, M., Janssen, P., Leckler, F., and Westhuysen, A.: User manual and system

1777   documentation of WAVEWATCH III (R) version 5.16, 2016.

1778 Turner, A., and Millward, G. E.: Suspended Particles: Their Role in Estuarine Biogeochemical Cycles,

1779   Estuarine, Coastal and Shelf Science, 55, 857-883, 10.1006/ecss.2002.1033, 2002.

1780 van der Wegen, M., Dastgheib, A., Jaffe, B. E., and Roelvink, D.: Bed composition generation for

1781   morphodynamic modeling: case study of San Pablo Bay in California, USA, Ocean Dynamics, 61,

1782   173-186, 10.1007/s10236-010-0314-2, 2010.

1783 Walsh, J. P., and Nittrouer, C. A.: Understanding fine-grained river-sediment dispersal on continental

1784   margins, Marine Geology, 263, 34-45, 10.1016/j.margeo.2009.03.016, 2009.

1785 Wang, C., Li, W., Chen, S., Li, D., Wang, D., and Liu, J.: The spatial and temporal variation of total

1786   suspended solid concentration in Pearl River Estuary during 1987-2015 based on remote sensing,

1787   Science of The Total Environment, 618, 1125-1138, 10.1016/j.scitotenv.2017.09.196, 2018.

1788   Wang, C., Liu, Z., Harris, C. K., Wu, X., Wang, H., Bian, C., Bi, N., Duan, H., and Xu, J.: The Impact

1789   of Winter Storms on Sediment Transport Through a Narrow Strait, Bohai, China, Journal of

1790   Geophysical Research: Oceans, 125, e2020JC016069, https://doi.org/10.1029/2020JC016069,

1791   2020.

1792   Wang, S., Zhang, N., Chen, H., Li, L., and Yan, W.: The surface sediment types and their rare earth

1793   element characteristics from the continental shelf of the northern south China sea, Continental

1794   Shelf Research, 88, 185-202, 10.1016/j.csr.2014.08.005, 2014.

1795   Wang, S., Wu, S., Yan, W., Huang, W., Miao, L., Lu, J., Chen, Z., and Liu, F.: Rare metal elements in

1796   surface sediment from five bays on the northeastern coast of the South China Sea, Environmental

1797   Earth Sciences, 74, 4961-4971, 10.1007/s12665-015-4504-6, 2015.

1798   Wang, S., Li, J., Wu, S., Yan, W., Huang, W., Miao, L., and Chen, Z.: The distribution characteristics of

1799   rare metal elements in surface sediments from four coastal bays on the northwestern South China

1800   Sea, Estuarine, Coastal and Shelf Science, 169, 106-118, 10.1016/j.ecss.2015.12.001, 2016.

1801   Wang, Y., Wang, Y., Wan, X., Huang, C., Wang, R., Liu, X., Yi, J., and Zhang, Y.: Influence of the

1802   Hanjiang River's Inlet Sediment Decrease on Modern Sedimentation in the Underwater Delta,

1803   Applied Sciences, 13, 8039, 10.3390/app13148039, 2023.

1804   Warner, J. C., Sherwood, C. R., Arango, H. G., and Signell, R. P.: Performance of four turbulence

1805   closure models implemented using a generic length scale method, Ocean Modelling, 8, 81-113,

1806   10.1016/j.ocemod.2003.12.003, 2005.

1807   Warner, J. C., Sherwood, C. R., Signell, R. P., Harris, C. K., and Arango, H. G.: Development of a

1808   three-dimensional, regional, coupled wave, current, and sediment-transport model, Computers &

1809   Geosciences, 34, 1284-1306, 10.1016/j.cageo.2008.02.012, 2008.

1810   Warner, J. C., Armstrong, B., He, R., and Zambon, J. B.: Development of a Coupled

1811   Ocean–Atmosphere–Wave–Sediment Transport (COAWST) Modeling System, Ocean Modelling,

1812   35, 230-244, 10.1016/j.ocemod.2010.07.010, 2010.

1813   Warner, J. C., Schwab, W. C., List, J. H., Safak, I., Liste, M., and Baldwin, W.: Inner-shelf ocean

1814   dynamics and seafloor morphologic changes during Hurricane Sandy, Continental Shelf Research,

1815   138, 1-18, 10.1016/j.csr.2017.02.003, 2017.

1816   Weatherall, P., Marks, K. M., Jakobsson, M., Schmitt, T., Tani, S., Arndt, J. E., Rovere, M., Chayes, D.,

Ferrini, V., and Wigley, R.: A new digital bathymetric model of the world's oceans, Earth and Space Science, 2, 331-345, https://doi.org/10.1002/2015EA000107, 2015.

Wright, L. D., and Coleman, J. M.: Variations in Morphology of Major River Deltas as Functions of Ocean Wave and River Discharge Regimes, AAPG Bulletin, 57, 370-398, 1973.

Wright, L. D., and Nittrouer, C. A.: Dispersal of river sediments in coastal seas: Six contrasting cases, Estuaries, 18, 494-508, 10.2307/1352367, 1995.

Wu, C., Xing, W., Jie, R., Yun, B., Zhigang, H., Yiaping, L., Heyin, S., and Wenyan, Z.: Morphodynamics of the rock-bound outlets of the Pearl River estuary, South China — A preliminary study, Journal of Marine Systems, 82, S17-S27, 10.1016/j.jmarsys.2010.02.002, 2010.

Wu, Z., Milliman, J. D., Zhao, D., Zhou, J., and Yao, C.: Recent geomorphic change in LingDing Bay, China, in response to economic and urban growth on the Pearl River Delta, Southern China, Global and Planetary Change, 123, 1-12, 10.1016/j.gloplacha.2014.10.009, 2014.

Wu, Z., Milliman, J. D., Zhao, D., Cao, Z., Zhou, J., and Zhou, C.: Geomorphologic changes in the lower Pearl River Delta, 1850–2015, largely due to human activity, Geomorphology, 314, 42-54, 10.1016/j.geomorph.2018.05.001, 2018.

Wu, Z. Y., Saito, Y., Zhao, D. N., Zhou, J. Q., Cao, Z. Y., Li, S. J., Shang, J. H., and Liang, Y. Y.: Impact of human activities on subaqueous topographic change in Lingding Bay of the Pearl River estuary, China, during 1955-2013, Scientific Reports, 6, 37742, 10.1038/srep37742, 2016.

Xia, X. M., Li, Y., Yang, H., Wu, C. Y., Sing, T. H., and Pong, H. K.: Observations on the size and settling velocity distributions of suspended sediment in the Pearl River Estuary, China, Continental Shelf Research, 24, 1809-1826, 10.1016/j.csr.2004.06.009, 2004.

Xu, K., Corbett, D. R., Walsh, J. P., Young, D., Briggs, K. B., Cartwright, G. M., Friedrichs, C. T., Harris, C. K., Mickey, R. C., and Mitra, S.: Seabed erodibility variations on the Louisiana continental shelf before and after the 2011 Mississippi River flood, Estuarine, Coastal and Shelf Science, 149, 283-293, https://doi.org/10.1016/j.ecss.2014.09.002, 2014.

Xu, K., Mickey, R. C., Chen, Q., Harris, C. K., Hetland, R. D., Hu, K., and Wang, J.: Shelf sediment transport during hurricanes Katrina and Rita, Computers & Geosciences, 90, 24-39, https://doi.org/10.1016/j.cageo.2015.10.009, 2016.

Xue, Z., He, R., Liu, J. P., and Warner, J. C.: Modeling transport and deposition of the Mekong River

sediment, Continental Shelf Research, 37, 66-78, 10.1016/j.csr.2012.02.010, 2012.

Yang, B., Liu, S.-M., and Zhang, G.-L.: Geochemical characteristics of phosphorus in surface sediments from the continental shelf region of the northern South China Sea, Marine Chemistry, 198, 44-55, 10.1016/j.marchem.2017.11.001, 2018.

Yang, J., Wu, D., and Lin, X.: On the dynamics of the South China Sea Warm Current, Journal of Geophysical Research: Oceans, 113, https://doi.org/10.1029/2007JC004427, 2008.

Young, I. R., Zieger, S., and Babanin, A. V.: Global trends in wind speed and wave height, Science, 332, 451-455, 10.1126/science.1197219, 2011.

Zang, Z., Xue, Z. G., Xu, K., Bentley, S. J., Chen, Q., D'Sa, E. J., and Ge, Q.: A Two Decadal (1993–2012) Numerical Assessment of Sediment Dynamics in the Northern Gulf of Mexico, Water, 11, 938, 2019.

Zeng, X., He, R., Xue, Z., Wang, H., Wang, Y., Yao, Z., Guan, W., and Warrillow, J.: River-derived sediment suspension and transport in the Bohai, Yellow, and East China Seas: A preliminary modeling study, Continental Shelf Research, 111, 112-125, https://doi.org/10.1016/j.csr.2015.08.015, 2015.

Zhan, W., Wu, J., Wei, X., Tang, S., and Zhan, H.: Spatio-temporal variation of the suspended sediment concentration in the Pearl River Estuary observed by MODIS during 2003–2015, Continental Shelf Research, 172, 22-32, 10.1016/j.csr.2018.11.007, 2019.

Zhang, G., Cheng, W., Chen, L., Zhang, H., and Gong, W.: Transport of riverine sediment from different outlets in the Pearl River Estuary during the wet season, Marine Geology, 415, 105957, 10.1016/j.margeo.2019.06.002, 2019.

Zhang, G., Chen, Y., Cheng, W., Zhang, H., and Gong, W.: Wave Effects on Sediment Transport and Entrapment in a Channel-Shoal Estuary: The Pearl River Estuary in the Dry Winter Season, Journal of Geophysical Research: Oceans, 126, 10.1029/2020jc016905, 2021.

Zhang, G., Hu, P., Hu, S., Zhang, H., and Gong, W.: Tidal effects on the dispersal and water age of the plumes from eight outlets of the Pearl river during the wet summer, Ocean & Coastal Management, 266, 107704, https://doi.org/10.1016/j.ocecoaman.2025.107704, 2025.

Zhang, J., Jiang, Q., Jeng, D., Zhang, C., Chen, X., and Wang, L.: Experimental Study on Mechanism of Wave-Induced Liquefaction of Sand-Clay Seabed, Journal of Marine Science and Engineering,

1875   8, 66, 10.3390/jmse8020066, 2020.

1876   Zhang, W., Wei, X., Zheng, J., Zhu, Y., and Zhang, Y.: Estimating suspended sediment loads in the

1877   Pearl River Delta region using sediment rating curves, Continental Shelf Research, 38, 35-46,

1878   10.1016/j.csr.2012.02.017, 2012.

1879   Zhang, W., Zheng, J., Ji, X., Hoitink, A. J. F., van der Vegt, M., and Zhu, Y.: Surficial sediment

1880   distribution and the associated net sediment transport pattern retain-->in the Pearl River Estuary,

1881   South China, Continental Shelf Research, 61-62, 41-51, 10.1016/j.csr.2013.04.011, 2013.

1882   Zhang, Y. J., Ye, F., Stanev, E. V., and Grashorn, S.: Seamless cross-scale modeling with SCHISM,

1883   Ocean Modelling, 102, 64-81, https://doi.org/10.1016/j.ocemod.2016.05.002, 2016.

1884   Zhong, Y., Chen, Z., Li, L., Liu, J., Li, G., Zheng, X., Wang, S., and Mo, A.: Bottom water

1885   hydrodynamic provinces and transport patterns of the northern South China Sea: Evidence from

1886   grain size of the terrigenous sediments, Continental Shelf Research, 140, 11-26,

1887   10.1016/j.csr.2017.01.023, 2017.

1888   Zong, X., Cheng, X., Zhang, S., Lian, Q., Deng, F., and Chen, Z.: Tidal effects on dynamics and

1889   freshwater transport of a medium-scale river plume with multiple outlets, Ocean Modelling, 188,

1890   102338, https://doi.org/10.1016/j.ocemod.2024.102338, 2024.

1891   Zong, Y., Huang, K., Switzer, A., yu, F., and Yim, W.: An evolutionary model for the Holocene

1892   formation of the Pearl River delta, China, The Holocene, 19, 129-142,

1893   10.1177/0959683608098957, 2009.

1894